POLITECNICO DI MILANO

Facoltà di Ingegneria Meccanica

Master of Science in

Mechanical Engineering

FABRICATION AND EVALUATION OF LAB-ON-A-CHIP MICROFEATURES BY DLP-STEREOLITHOGRAPHY

Supervisor: Prof. Irene Fassi

Co-Supervisor: Dr. Lara Rebaioli

MSc. Thesis of:

Mallarapu Nagarjun,

Id:10604659

Moosa Kaleemullah Syed,

Id:10601185

Academic Year 2019 – 2020

ACKNOWLEDGEMENT

We would like to sincerely express our gratitude towards Prof. Irene Fassi and thank her for supporting us in the completion of our Thesis work. Throughout the thesis work, she was constantly guiding us and providing her support, with her immense knowledge in the field of engineering and research.

Besides our supervisor, we would like to thank the Co-Supervisor Dr. Lara Rebaioli, for providing the necessary support, and guiding us in theoretical as well as practical work.

We also like to express our gratitude towards the National Research Council of Italy CNR-STIIMA, for providing the necessary lab and machine for experimenting and arranging the technical staff whenever needed.

Further, we would like to especially thank all the faculty and staff members of the Department of Mechanical Engineering to deliver in-depth knowledge in the field of Mechanical Engineering throughout our period of being a student.

Lastly, we would like to thank parents and family members for virtually being with us every time although not physically present and most importantly supporting us mentally and emotionally throughout our Masters.

ABSTRACT

In recent years, with the advent of microfluidics, several advancements in the field of science are being made. Thus, the design of microfluidics is continuously evolving to be more and more complex. Soft lithography cannot be used for complex and advanced applications because of its limitations for the design complexity, the time involved, the labor involved, the space requirements and the commercialization. This made the researchers think of a cutting-edge technology that could provide an optimal solution to the above-stated limitations. To suit several advanced applications, which cannot be readily produced by the conventional methods, the development of a 3D printing or Additive Manufacturing (AM) technology, such as DLP (Digital Light Processing) Stereolithography process is a solution. This technology apart from addressing the above-stated limitations also provides a good resolution and complex topology solution. This thesis aims at designing a new benchmark artifact to evaluate the capability as well as the performance of a DLP Stereolithography system, for the manufacturing of 3D-complex microfluidic features. The proposed benchmark artifact includes several planar and non-planar channels along with several complex geometries and cross-sections, like that of several lab-on-chip applications and few of the previously designed benchmark artifacts.

TABLE OF CONTENTS

LIST OF FIGURES

LIST OF TABLES

INTRODUCTION

Lab on-chip devices (LOCs) are miniaturized devices that are based on microfluidics. These devices aid in performing several complex analyses on a single chip. They are rapidly spreading and are widely used technology enabling easier analysis, and are applied in several fields of chemical, biological, and environmental importance.

Low infrastructure costs and ease of manufacturing has led to the usage of polydimethylsiloxane (PDMS) and soft lithography in the manufacturing of lab on chip devices LOCs. However, these fabrication approaches are limited by the range of features that can be created, with a move from 2.5 dimensional (structures with varying width but identical depth) to 3-dimensional structures that can increase the processing cost thus reducing the success rates. Moreover, these techniques require much space to hold multiple pieces of equipment, labour and are multiple-step processes to make final product thus cause time wastage, when making a change in design, and suffer from the limited availability of biological materials.

The additive manufacturing (AM) processes enable the manipulation of surfaces and fluids in three dimensions. These processes use a material that is more like thermoplastics. Few three-dimensional structures are impossible or more challenging to make with existing approaches. The additive manufacturing (AM) process can create truly three-dimensional structures that will provide a new microfluidic capability.

Among the available additive manufacturing (AM) processes, stereolithography is a promising technique to produce microfluidic devices with micro features, high accuracy, and surface finish. However, this additive manufacturing (AM) Technology also faces certain challenges and barriers for its applicability. The additive manufacturing (AM) technology cannot currently compete with the resolution of the structures that are produced by conventional lithography in a build space. There are also few concerns regarding the shape conformity, dimensional fidelity, surface quality, material biocompatibility, optical transparency, and availability.

The resolution is limited by both the properties of the resin and the physical resolution of the laser-projection system. The hardware resolution is not the main limitation but achieving this within a reasonable time frame with a usable build space for microfluidics is a concern. Apart from this, the Stereolithography process is restricted to single print at a time and all the photopolymers utilized were highly toxic.

The main objective of the thesis is to design a benchmark artifact with complex geometries as well as cross-sections to investigate a lab-on-chip (LOC) manufacturing by Digital Light Processing (DLP) Stereolithography process. The proposed design is based on channel sections and designs of literature reviews on the benchmark artifacts along with typical features of microfluidic devices. Moreover, the artifact is designed based on the results of a preliminary experimental campaign performed on the artifact proposed by a bachelor thesis "Studio preliminare della fattibilità dell'ultra-fast prototyping di Lab-on-Chips mediante stereolitografia".

Chapter 1 deals with the literature review that has allowed us to define the thesis objectives. It includes a brief introduction to lab-on-chip (LOC), current manufacturing techniques, additive manufacturing (AM) Technology , Stereolithography (SLA) process and configurations, advantages, challenges and the limitations of the Stereolithography (SLA) process ,materials used for fabrication for microfluidics, existing artifacts made from Stereolithography (SLA) process along with the certain microfluidic applications of different geometries and cross-sections which laid the foundation to propose a benchmark artifact .This chapter also draws the thesis objectives.

Chapter 2 deals with the preliminary experimental campaign based on the artifact proposed by a bachelor thesis "Studio preliminare della fattibilità dell'ultra-fast prototyping di Lab-on-Chips mediante stereolitografia". A detailed qualitative and ANOVA analysis is also included in this chapter.

Having seen the literature review and the preliminary experimental campaign the new proposed benchmark artifact with complex planar and nonplanar channels, 3D helical channels is described and discussed in Chapter 3.

Finally, the conclusion and the future development of this study are discussed in Chapter 4.

CHAPTER 1

LIETRATURE REVIEW

1. LITERATURE REVIEW

1.1 LAB-ON-A-CHIP

The advent of micromanufacturing technologies has given the path to a tremendous increase in investment in the field of science and technology. Microfluidic devices or in other words “lab-on-a-chip” are the devices used mostly in biomedical applications. They are generally used to handle and analyse the microfluidics in the micrometre scale. They also can combine several laboratory functions onto a single chip which gives them a significant advantage [1].

Some of the key functions of these devices are sample preparation, separation, detection, and fluid manipulation. Different functional components can be incorporated on a single chip and each of these plays a different role. for liquid handling, the range of the cross-section of these devices varies from 1 to 500 μm and small volume capacity (femtoliters or picolitres) [2]. Many applications of microfluidics are used in biology studies, such as testing to point-of-care (directly at the point of patient care), the analysis of single cells and nucleic acids, or the discovery of new drugs.

1.2 MANUFACTURING PROCESSES

Nowadays, different techniques in fabricating microfluidic devices both in large-scale and small-scale production such as micro-manufacturing, soft-lithography, injection molding, inkjet, fused deposition modelling (FDM), two-photon polymerization (2PP), and Stereolithography (SLA), etc are available. Some of these processes take much time, space to hold and few are multiple-step processes to make the final product. For the inkjet, the main limitations are the difficulty in the removal of the support material from the channels and the limited availability of biocompatible and transparent materials, which are necessary for microfluidic devices. The fused deposition modelling (FDM), while being inexpensive and easy to use, presents surface finishes and dimensional accuracy too inaccurate to produce LOC. The 2PP may be the best choice in terms of dimensional accuracy, however, cannot be applied for rapid prototyping due to the large process time, the high cost of laser and optical positioning devices, and the absolute need for a vacuum chamber [3,4].

In general, in small scale production, soft lithography is used. Most microfluidic devices are constructed by this soft lithography, using materials such as Polymethyl methacrylate (PMMA) and especially the polydimethylsiloxane (PDMS), a biocompatible material, transparent,

elastomeric and gas permeable. This is a quick and easy fabrication process, but it is a multiple-step process [1, 2]. Although these are very inexpensive materials, not to mention that this method is capable of printing only in 2.5D and requires specialized personnel.

A rapid increase in the additive manufacturing (AM)process helps to fabricate the Lab-on-a-chip devices in a single step process without the need for assembly, quickly and even the complex entity [3].

3Dimensional printing or additive manufacturing of is a manufacturing process in which an object is created by layer by layer joining of a 3Dimensional model data. Two-photon polymerization, inkjet, Stereolithography, and fused deposition modelling are the extensively employed additive manufacturing (AM)processes in microfluidics development. The choice of the most suitable technique employed for the production is a function of the definition of the purpose which can be aesthetic, functional or investigational [5,6].

However, amongst all the processes, Stereolithography strikes a perfect balance between resolution, price, and performance, thus making it a very attractive option for microfluidics manufacturing. These printers are employed with varying resolution in both XY and Z. The factors affecting the machine of choice are the resolution (accuracy), speed, material and build size [5,6].

1.3 STEREOLITHOGRAPHY

To tackle rapid prototyping bottlenecks and in a quest of quick and superior design needs, the Stereolithography process was developed simultaneously in France (CNRS- July 84.French Patent N’84 11 241) and in USA (U.V.P- C. HULL Aug, 84. US Patent N 45 75 220). In this process, a liquid photosensitive polymer (also known as resin) undergoes an exothermic polymerization process characterized by chemical cross-linking reactions during curing or solidification reaction, resulting in a highly cross-linked 3D network which is insoluble and infusible, when a UV light source of a proper amount of energy introduced over its surface [7].

This amount of energy that is being introduced to initiate the curing or solidification reaction is the function of the selected Stereolithography technique [8,9].

The entire Stereolithography process to create a 3D part or a structure involves an input data, a part preparation, the layer preparation, and finally formation and stacking of 2 dimensional

cross-sectional slices. This method is being employed in microfluidics as the polymerization of the walls of the channel cavities with subsequently draining the uncured photopolymer precursor results in the formation of microchannels without the use of any bonding or alignment creating very fine features in a rapid manner [6,11,12].

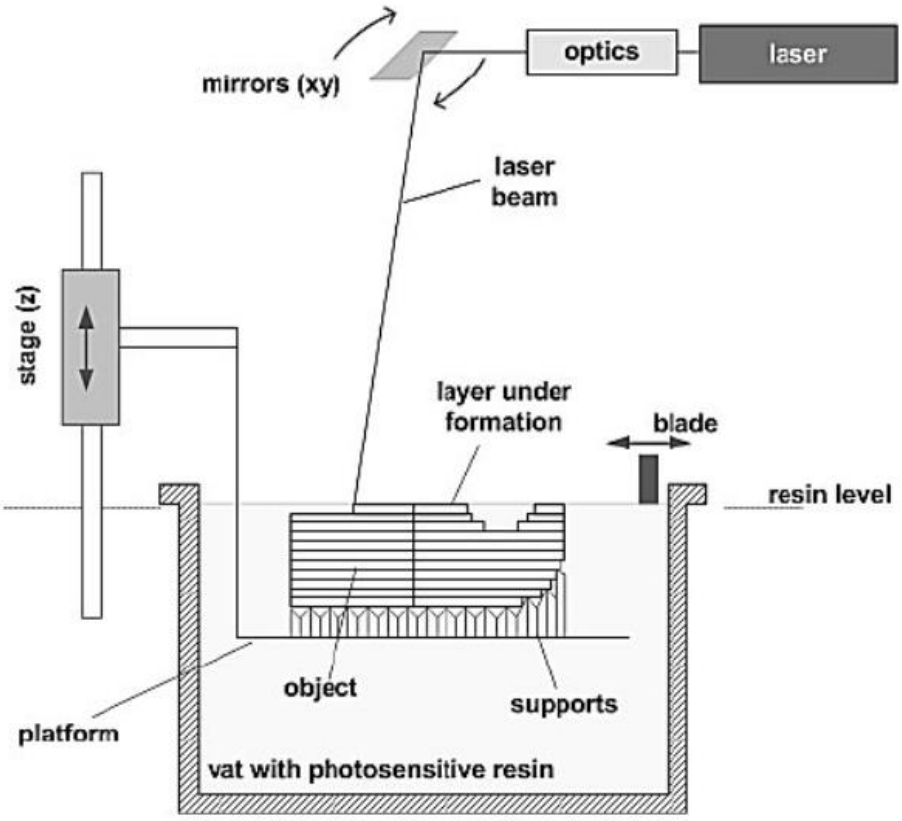

Figure 1 Stereolithography Process [11].

1.3.1 PROCESS

3-dimensional Systems company introduced its Stereolithography machines for industrial product production. Commercial photopolymers can be cured by various forms of radiation, including electron beams, X-rays, gamma rays, ultraviolet, and visible light. Mainly, the ultraviolet and visible light radiation is used in Stereolithography systems for curing purposes. The method of creating a model using the digital light processing stereolithography apparatus consists of a series of steps. Firstly, design of a CAD layout of the chip in a 3d software. After this, the CAD layout is exported into an STL format. If necessary, the support framework can be added. Further steps are, the specification of variables and parameters of the building style required for the slicing, slicing a machine model to produce the information regulating it,

Construction of a 3 dimensional a component using sliced material, Post-treatment, post curing (where necessary). The general flowchart of the process was listed below in figure 3 [13].

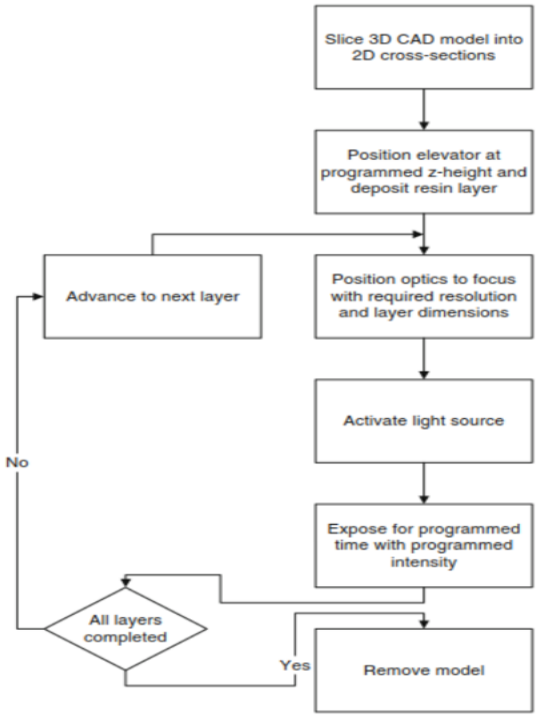

Figure 2 Stereolithography construct phase flowchart [13].

The CAD model of the desired part is sliced so that the layers can be integrated to form parts from a resin that is either acrylic or epoxy in nature. The bottommost feature or surface in the model is the one that forms first. Then the building process moves upward to form an object or part. This upward building is due to the lowering of the elevator into the vat of resin. This lowering movement is carried out according to the specified layer thickness. The current layer or next layer will be drawn at the surface of the vat as it descends downwards focussed on the 3D solid model. The layers are assembled as energy is induced on them curing a cross-section of contours in the x-y axis. The scanned resin is solid plastic by the cross-linking of excited resin polymers-photopolymerization (Paul F. Jacobs 1992). Once a substrate has been screened, the platform will lower after scanning a line, and the next "strip" will be cured and bound to the prior one (the line below the new one). This bonding is triggered by hatching over cure. Of successive layers, the cycle repeats itself until the top layer (constituting the highest point on the component, considering the direction of the model) is cured and the portion is complete [14].

The initial layer is not the first stage of curing that occurs in the process. Tiny structures that measure approximately 0.4in in height called “supports.” These supports prevent the bottom surface of the part from being cured directly on the platform. They can also ease the process of removing parts from the platform and aid in preserving most of the parts. The surfaces that face downward, concerning the build direction are “down-facing surfaces.” and the contrary to this are the “up-facing surfaces.” The main reason for the support is for protecting most of the surface’s finish. The supports can be removed easily after the completion of post-curing. After removing the supports, they can leave tiny “bumps” from where they once made contact. To main the geometric integrity of the part, these supports also are mainly used. The thin or overhanging features can collapse if additional strength is applied. The collapse may be due to their weight or the applied weight of the free resin. After the part is built, it is ready for the post-processing phase. This phase includes cleaning, post-curing, and finishing the part [14].

1.3.2 STEREOLITHOGRAPHY CONFIGURATIONS

1.3.2.1 SLA SCANNING MODE

This process (Fig 3A) is carried out by a spatially controlled point laser. The photopolymerization of liquid resin is carried out when the point laser scans over the resin. Thus, selectively cures and solidifies the cross-section of an object inside the build area resulting in the formation of the object building up layer by layer. The disadvantage of these types of 3D printing technologies that is using a point laser is that it would take much longer timer in tracing the cross-section of an object [15].

1.3.2.2 DIGITAL LIGHT PROCESSING (DLP):

Another process is the Digital light processing technique (DLP). This process carries out using a digital light projector. The digital light projector is a digital screen, that uses the flash of a single image which cures the layer all at once that leads to shorter production times when compared to the other configuration of Stereolithography process [15]. Each layer of the image consists of square pixels. These square pixels create a small rectangular block called voxels.

The present study focuses on designing a benchmark artifact that consists of micro features and channels that is produced by a Digital light processing technique (DLP) system.

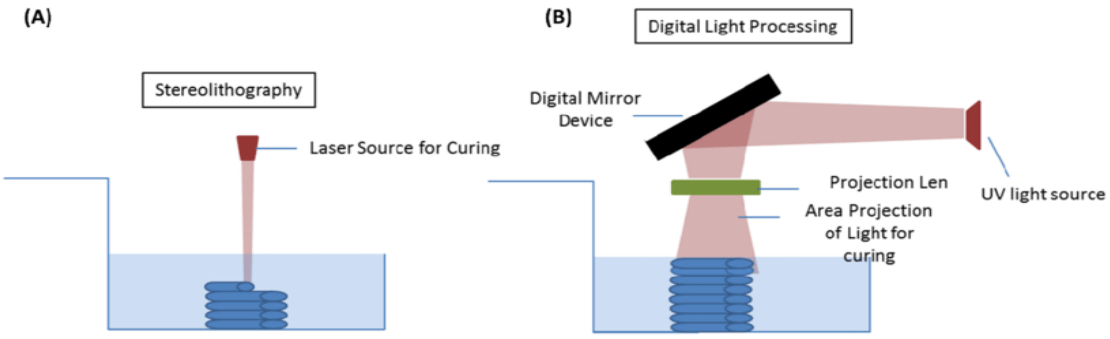

Figure 3 Scheme of two types of Stereolithography left: SLA scanning mode right: Digital light processing [15]

1.3.3 ADVANTAGES OF STEREOLITHOGRAPHY

Stereolithography is a flexible production process, which is very easy to understand, and which aids in the creation of Complex Structures, with a High Resolution and precision in a single-step with Low production time without the need of an assembly and any skilful labor. It employs a wide scope of biomaterials hence aids in several biomedical applications. It is a low-cost procedure as it uses very little material for fabrication. Its Standardized procedure where a part can be shared with and moved to any lab that has a CAD program and 3D printer. It also helps to improve the design and structure of existing chips by promoting the manufacture of Microfluidics Interface. Moreover, the Stereolithography apparatus is small and requires very little space. The Stereolithography manufactured parts can be extended to produce a higher-order multiple emulsion with more compartments, thus aiding in applications such as drug delivery, food, cosmetics, and materials science [20].

1.3.4 CHALLENGES AND LIMITATIONS

Resin being photosensitive creates handling issues: Resin handling is one of the main concerns when dealing with Stereolithography (SLA) as the resin must be handled in an appropriate way to prevent it from curing before the start of the process. This may mean that molding must be carried out in darkened or shaded areas or even include covered sections to prevent the resin from becoming affected. Another major drawback of the Stereolithography process is having a limited number of resins that are commercially available for processing, which restricts its extension to various applications [6].

Limited availability of Resin is a major concern. The major drawback of the Stereolithography process is having the limited number of resins, that are commercially available for processing, which restricts its extension to various applications [6].

Restriction of the process to single print material at a time: The Stereolithography process is restricted to the usage of one resin at a time. The capacity to stack up multiple resins is quite feasible but the complex sequential polymerization and rinsing steps are required for each integrated layer. A big technical obstacle resides in the creation of an integrated resin removal device and resin exchange reservoirs. The prohibition on using one resin in the Stereolithography is probably the main concern [25].

Other Limitations. The Stereolithography built parts, are not on par with the conventional lithography in terms of resolution in a build space. However, the hardware resolution isn't the main concern, but achieving this with a usable build space for microfluidics within a reasonable timeframe is an issue. There are also other issues of dimensional fidelity, shape conformity, surface quality, biocompatibility, and optical transparency [6].

1.4 MATERIAL

The first-generation microfluidic device materials used were glass and silicon. However, owing to their high cost they were soon replaced by Elastomers. This has enabled low-cost rapid prototyping with a high-density integration of valves on the chip promoting a complicated as well as parallel fluid manipulation with in-channel cell culture. Later several other materials such as thermoplastics, due to their similarity in advantages to that of elastomer, were used.

Apart from this, the thermoset supports were utilized for the fabrication of arbitrary 3D structures. Hydrogels, due to its high permeability that has enabled the diffusion of molecules without bulk fluid flows were used by chemists, and the per-Fluro-polymers which were inert, and antifouling was also utilized. Thus, several materials were used to suit a variety of microfluidic applications for their distinct characteristics. Recently paper-based devices were introduced, which are extremely low-cost to prepare and easy to use, thereby promising in commercial point-of-care assays. However, the thermoplastics (e.g. polymethylmethacrylate - PMMA, polycarbonate – PC, etc.) and soft elastomers (e.g. Polydimethylsiloxane - PDMS) are mostly used materials for LOC fabrication. Anyways a variety of materials have been developed to provide microfluidics with variable properties [16,17,18].

Most of Stereolithography resins, in general, are of are low-molecular-weight comprising of multi-functional monomers that undergo photopolymerization to form highly crosslinked networks. These materials are predominantly glassy, rigid, and brittle [19].

The general composition of resin consists of a Monomer, photo initiator, diluent/solvent, and photo absorber [10].

The photo initiator is activated by the light energy that is being incident on the resin. The resultant reactive species polymerize the monomers to form a solid crosslinked polymer network. Photo initiator optimizes the curing depth, as reduced curing depth would result in brittle structures, which would make the resultant unfit for medical applications. diluent/solvent reduces resin viscosity. The photo absorber controls light penetration depth. The base monomer selection tunes the biocompatibility and biodegradability properties, while the degree of crosslinking modifies the strength and elastic modulus of the final product. Thus, SLA printing is a function of Chemical composition, viscosity, and levelling of resin [19,20,21,22].

The first resins that were developed for the application in the Stereolithography process were polyacrylate or epoxy macromers with low molecular weights, which on being fed with the proper form of energy undergo a polymerization reaction thereby crosslinking to form a glassy network. However, these resins had issues about the high volumetric shrinkage, high distortion, and dimensional instability [23].

The preparation of elastomeric objects by Stereolithography is possible by few resins. These resins comprise of macromers having a low glass transition temperatures and comparatively higher molecular weights (1–5 kg/mol), with a non-reactive diluent such as N-methyl pyrrolidone (NMP) or water, which would reduce the viscosity of the resin [19].

The factors dictating the choice of the resin material for fabrication of an object using the Stereolithography process are the function, degree of integration, and the application of the object that is being fabricated by the process [10].

The choice of the type of resin also varies according to its properties such as biocompatibility, transparency, printability, viscosity, and elastic modulus. The transparency is necessary to allow printability and to observe the proper flow of liquids within the chip. The importance of

an appropriate viscosity is important due to the need to remove any cured resin not remained within the channels or at the junctions of the microchip. The biocompatibility of the material and its ability to absorb non-nucleic acids or proteins making it usable even in the biomedical field. Finally, the elastic modulus is essential to support the high pressures that are reached inside the microchannels.

Apart from the properties stated above, the resins can also possess the following properties such as oxygen inhibition capability to avoid any hindrance caused because of the oxygen during photopolymerization. The optimal critical energy to enable the photopolymerization process to take place at a supplied energy level to avoid curing at room temperatures. High dimensional stability to ensure that the material maintains its original dimensions when subjected to changes in temperature. Humidity, low volumetric shrinkage post-curing process, to avoid internal stresses and stresses at the margins of the restoration due to density change and volume reduction thus avoiding any marginal leakage. Secondary caries, optimal curing depth(using photo initiator) to avoid non-desirable brittle structures, cellular compatibility, solvent compatibility and supportability (oxygen, nutrient diffusion, etc.) to promote biomedical applications such as cell culture, tissue culture, etc [6,21,22,24,19,25,23].

With the development of technology and the advent of Stereolithography in various fields of science, diverse hybrid resins were fabricated using Proprietary epoxides and acrylate – epoxides. These resins have been characterized by having all the general properties, besides the increased layer integrity which provided strength, therefore paving a route to the manufacturing of an excessive-resolution Microfluidic Device [6,25,23].

1.5 EXISTING STUDIES OF THE MANUFACTURING OF MICROFLUIDIC DEVICES

Microfluidics has emerged to be a powerful tool in realizing an analysis, which is not only sensitive and fast but also fetches high throughput at a very low cost by manipulating fluids with the usage of channels and chamber structures which are microfabricated having cross-sections in the 1−500 μm range with a very small volume capacity, and which also be integrated with sensors and operators. It establishes an environment which is well controlled for manipulating fluids and particles, thereby paving its path to its implementation in both sophisticated chemicals as well as biological analyses with a low-cost point-of-care assay. In the scale of the micrometre, as distances of travel by mass and heat are relatively small, the reactions are fast thus are completed in a shorter amount of time while the flows are usually laminar with Reynolds number being low while the capillary effect being very dominant owing to large surface-to-volume ratios[6,7,8].

Each of the microfluidic devices is designed to serve a specific purpose; hence it comes with various geometries, cross-sections, channels, and therefore, designs. However, it has been observed that all geometries and cross-sections are the functions of their channels. They are several channels available, these channels are a function of the microfluidic applications, owing to their particle interaction and the flow [10].

The figure shown below fig (4), demonstrates monodisperse double emulsions with three-dimensional coaxially aligned cylindrical channels were made [28]. This kind of design was difficult to fabricate using conventional methods. By proper control of the flow at the inlet, the size, and the formation of the number of droplets can precisely be controlled. By adding more compartments, this process can be extended to generate higher-order multiple emulsions. Liquid photopolymer epoxy resin was used to fabricate the device and a UV laser beam was scanned over it. This method is mostly used in food, drug delivery, and cosmetics.

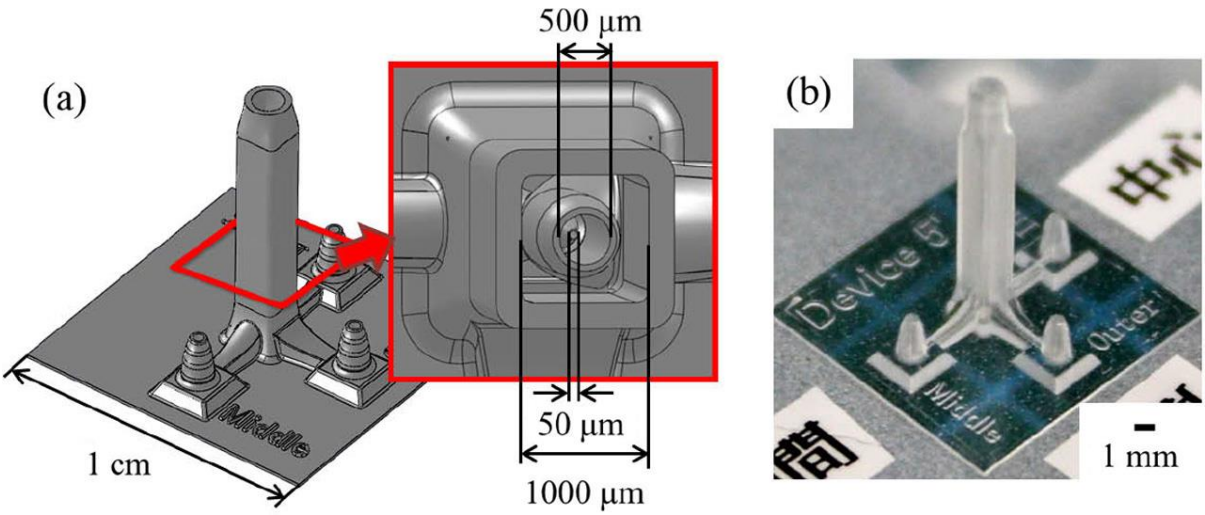

Figure 4 Monodisperse double emulsions with three-dimensional coaxially aligned cylindrical channels. Image is taken from the reference [28]

Another example of the preparation of the monodisperse complex three-dimensional microfluidic device was shown in the figure below (fig (5A), fig (5B), fig (5C)). This device consists of two coaxial channels with varying cross-section thus can generate water-in-oil emulsions at the third end [29]. An aqueous solution of a gelation reagent containing N-isopropyl acrylamide is used as a monomer, and the crosslinker is N, N'-methylene-bis-acrylamide (20mM). The photo initiator (0.3wt%, Ciba, DAROCUR 1173) was used. The droplets formation can precisely be controlled by managing the flow at the inlets.

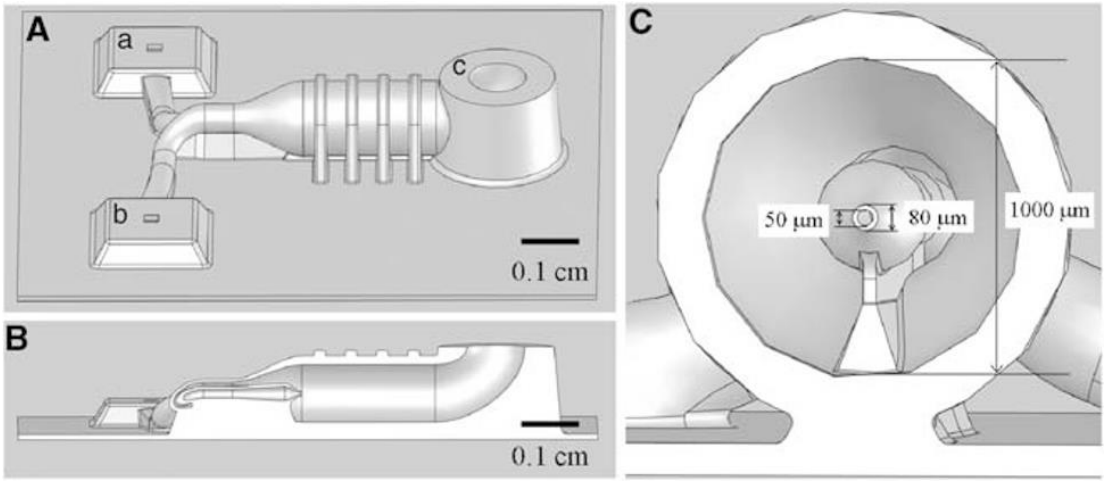

Figure 5 (A): A CAD model of the microfluidic device with coaxial flow geometry. 5(B): cross-sectional side view of the device with the channel axis at the centre. 5(C): A cross-sectional view of the device [29]

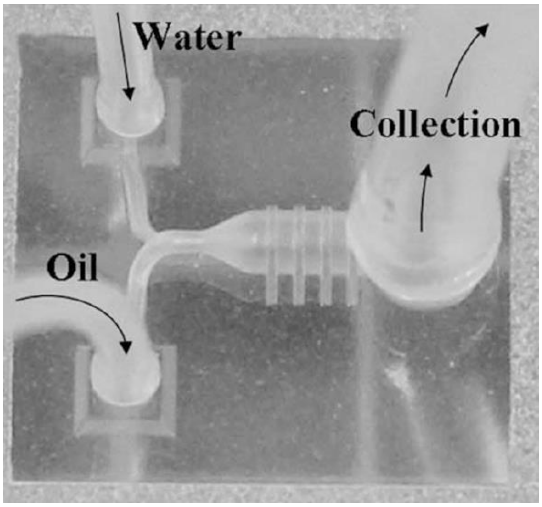

Figure 6 Photograph of the microfluidic device fabricated by Stereolithography. The length of a side of the square is 0.5mm. The image is taken from the reference [29].

The fig (7a) and fig (7b) illustrate a microfluidic fabricated using Stereolithography having axisymmetric flow focussing channels to produce various types of droplets and double emulsions. Here the fluid will not be in contact with the channels hence there is not any wetting or leakage issues. They are widely used in for applications that requiring small capsules such as in single cell encapsulation and the drug delivery systems. The material utilised is the photosensitive acrylates resin consisting of acrylic oligomer, pentaerythritol Penta acrylate, propylated and trimethylolpropane triacrylate [39].

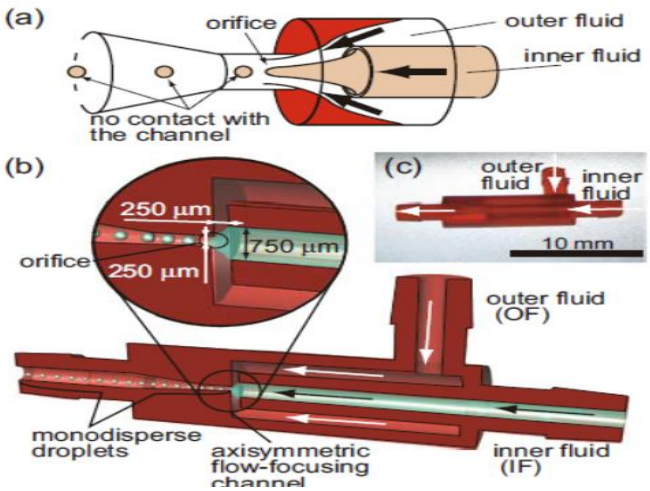

Figure 7 (a): The microfluidic device fabricated by Stereolithography in which the fluid in not in contact with the channel
Fig 7 (b): Axisymmetric flow focussing channels [39].

The most widely used channels in microfluidic systems are the straight microchannels, with rectangular or square cross-sections, as they are easy to fabricate, and have an ability for parallelization. The flows in these microchannels are dependent on two quantities: channel Re and particle Re. Thus, by manipulating these two dimensionless quantities, the flow can be varied. However, the flow within a straight microchannel is a function of its cross-section. The square cross-section has 4 focusing positions, which are altered to 2 when the cross-section is changed to rectangular (width/height=0.5). Generally, when the width to height ratio becomes high, stable focusing channels are reduced. However, with an increase of channel Re from a critical value, the stable equilibrium positions are increased, and they become a function of particle size, channel dimensions, and channel Re. flow cytometry applications are mainly exploited, with the usage of the straight microchannels [26].

Sinusoidal or serpentine microchannels have a better focusing performance, the ability of massive parallelization, with a small footprint. This better focusing performance is owing to the curvature direction changes in each loop, thus making them qualify for applications, involving a high-throughput separation for micron and sub-micron bioparticles (cyanobacteria) and harvesting of cyanobacteria. The equilibrium position of particles in these microchannels is the function of the flow rate and the focusing modes. Increase in the flow rate results in the defocusing of the particles flowing [26].

By altering the design from curvilinear to straight, a sinusoidal microchannel with a square-wave pattern is obtained which enables a size-based particle focusing with unique features.

The fig (8) demonstrates a microfluidic device with straight and serpentine microchannels which is most widely used in the biomedical field in the detection of the cancer cells separation in the blood samples. This operation is simple, takes less time, less sample and low cost [30]. The device is made of PDMS along with glass, later assembling the parts.

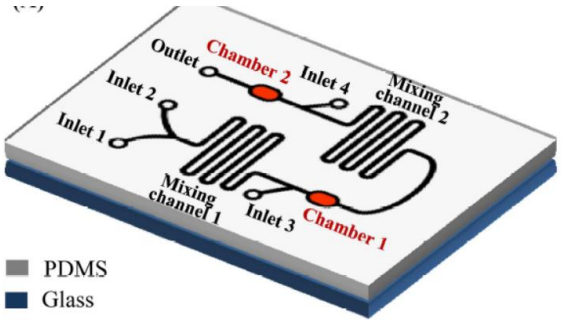

Figure 8 representation of the microfluidic chips with the serpentine feature [30].

Another example of the microfluidic device for the separation of the cancer cells in the blood sample is shown in the below fig (9) [31].

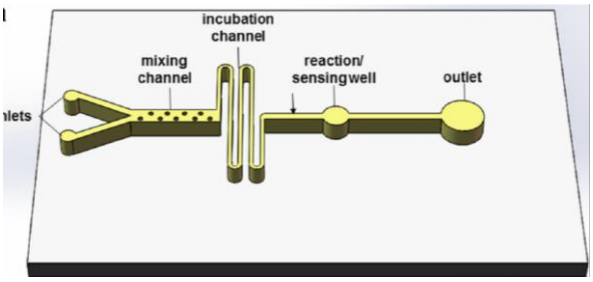

Figure 9 representation of the microfluidic chips with the serpentine feature [31].

Microfluidic shown in fig (10) is used in the formation of the emulsions, in drug delivery and cosmetics. In general, these devices are fabricated using the PDMS, and later assembling takes place [32].

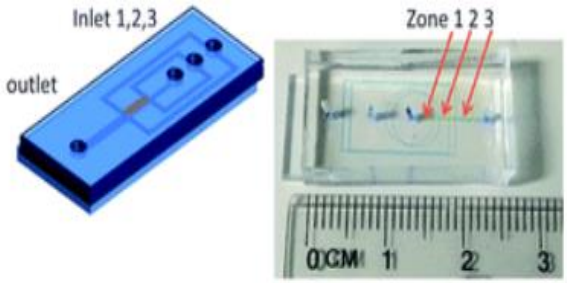

Figure 10 Microfluidic devices with circular channels and various cross-sections for the preparation of the emulsions [32].

As shown in the figure below (fig (11,12)), junctions are being utilised to make emulsions and cosmetics. By varying the inlet channel flow the output channel concentration can be varied [33,34].

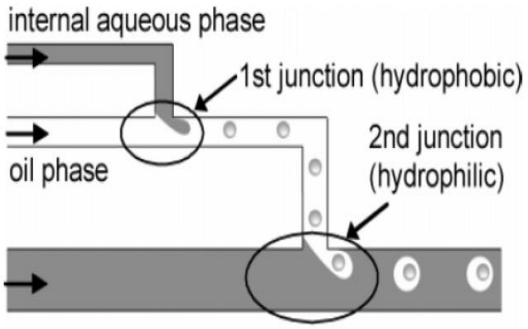

Figure 11 T junction [33]

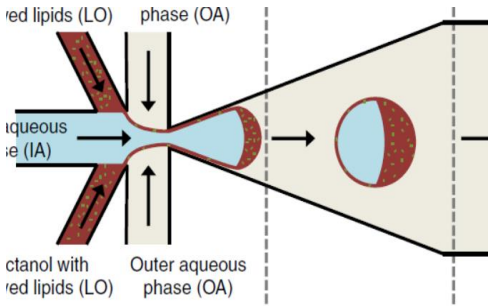

Figure 12 Y Junction [34]

Channels with a non-rectangular cross-section improve the fluid mixing in devices, operating at low Reynolds numbers (Re). The Nonplanar channels, when used at higher Re, induce an inertial focusing, thereby can be lending their way in several applications. Thus, by manipulating the Reynolds number, particle flow in the microfluidics can be exploited, suit the required application [10].

Microfluidics shown in fig (13), represent non-rectangular channels. They channels were utilised for internal focussing [35].

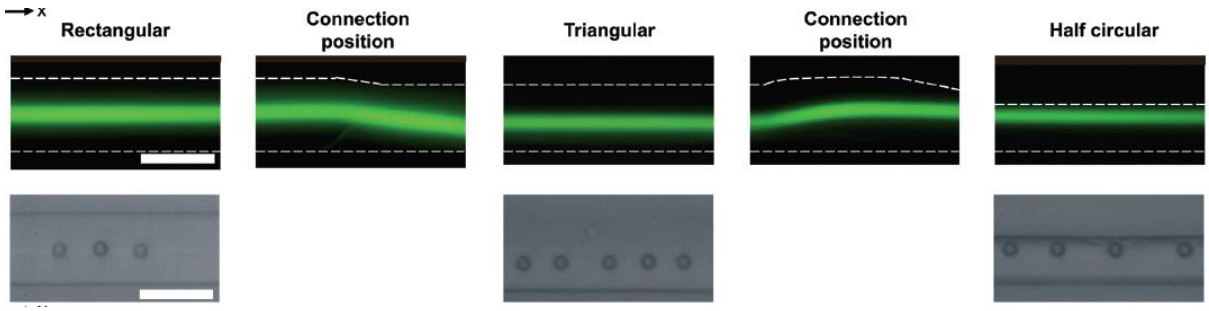

Figure 13 Representation of the non-rectangular channels in the microfluidic device [35]

The spiral microchannels are the ones, which aid in the particle sorting applications of microfluidics. These channels are characterized by a geometry that is defined as a curve winding channel around a center point with continuous decreasing or increasing manner. The flow that passes through the curvature, creates a velocity mismatch in the curve section of this channel, thereby generating secondary flows [26].

As shown in fig (14), microfluidics has the spiral microchannels. These channels are used to capture the bacteria when the sample is passing through the channel [36].

Figure 14 3D spiral non-planar channels [36]

Another example of the 3D nonplanar channels throughout the channel width is shown in the fig (15). A previous study was made on this type of channel using PDMS molding and casting.

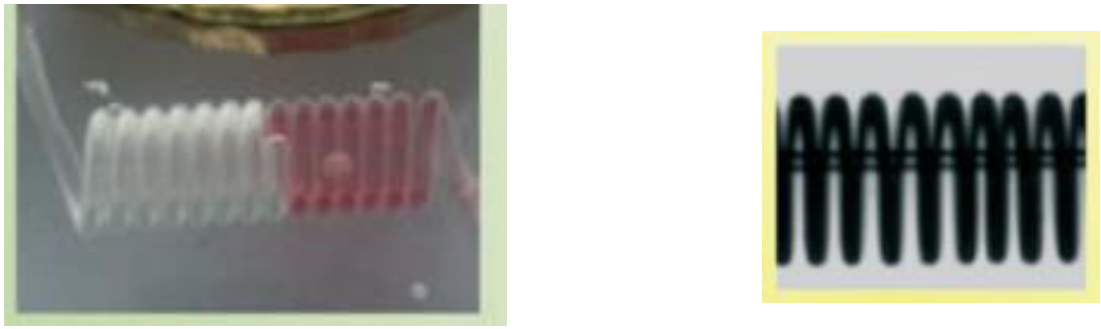

Figure 145 3D nonplanar channels throughout the channel length or width [36]

As shown in the fig (16) the 3D non-planar channels [40] used to form the emulsion that can be used in drugs and cosmetics. The complex 3D channel is also used in the separation of the blood samples. These channels gradually decrease in size, channel height, and width. By taking this below figure as a reference, the proposed benchmark artifact was made with complex nonplanar channels.

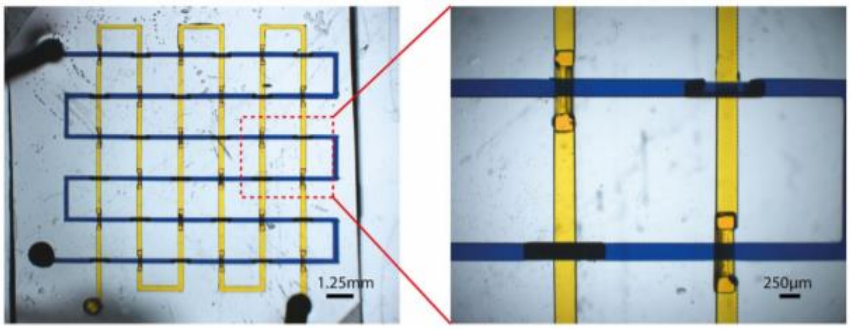

Figure 156 3D non-planar channels [40]

Microfluidics with complex channels is shown in figure (17). This complex channel structure is called bat-wing junction geometry, where there are 2 flows one being a middle flow and other being a side flow. Here in this complex geometry there is upstream and downstream intersection and bifurcation with expansion outlet and expansion zone with a staggered geometry. This bat-wing junction is utilized for the stepwise emulsification methods, to section a patterned first emulsion and later form a double emulsion droplet which are uniform, and which can encapsulate inner cores (droplets) of various dimensions and reagent composition. These chips are fabricated using polytetrafluoroethylene (PTFE) [37].

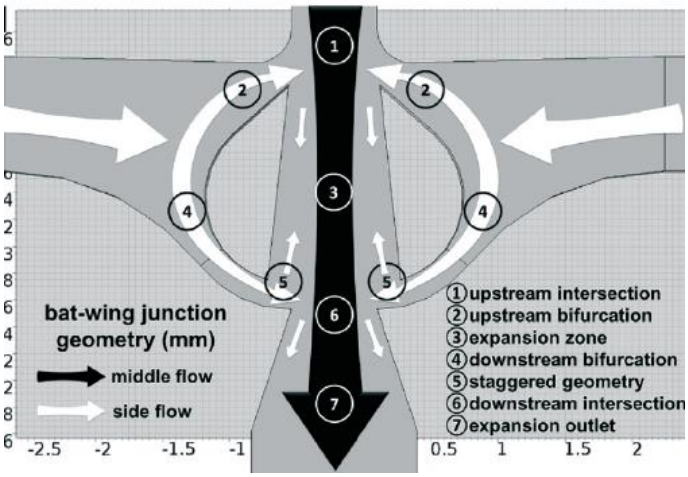

Figure 16 channels with Bat-wing junction [37].

1.5.1 EVALUATION OF MICROFEATURE MANUFACTURING BY DLP STEREOLITHGRAPHY

The fig (18) represents a benchmark artifact comprising of extrusions and intrusions of square and round sections, along with the spatial repeatability features [18]. These features are important to evaluate the geometrical performance of the Digital Light Projection (DLP) machine.

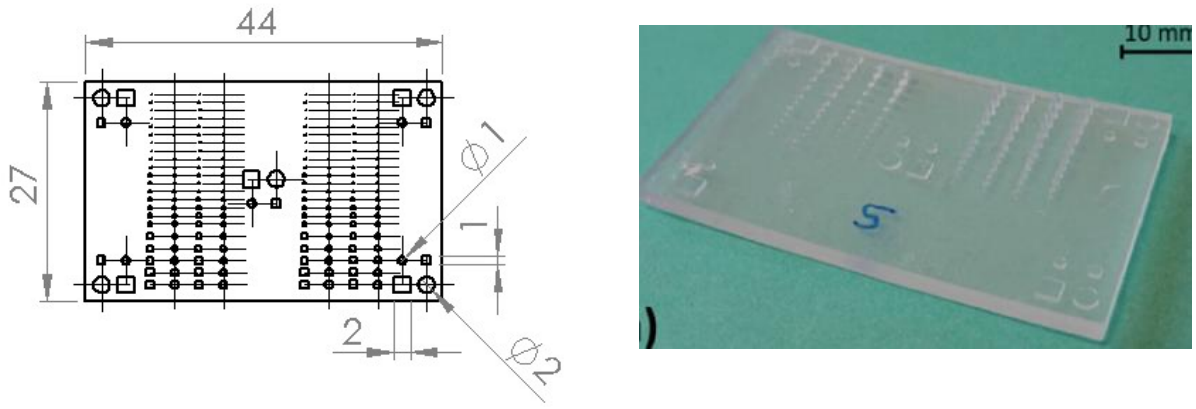

Figure 18: Intrusion/extrusion and the spatial repeatability features (left); artifact made by SLA process (right) [18].

Fig (19) illustrates a benchmark artifact proposed for the evaluation of the geometrical performance of a digital light processing Stereolithography(DLP-SLA) system to manufacture the microfeatures a benchmark artifact with positive (above the base surface) and negative features (below the base surface) and a detailed study was made [18]. In the experimental campaign, the effect of the main process parameters such as layer thickness and exposure time and the feature position within the build platform on the process parameters were specifically assessed and studied [18].

The benchmark artifact (fig 14B) was made using the DLP Stereolithography machine. The resin used is EnvisionTEC E-shell resin. This is water clear, transparent, and photocuring methacrylic/acrylic resin.

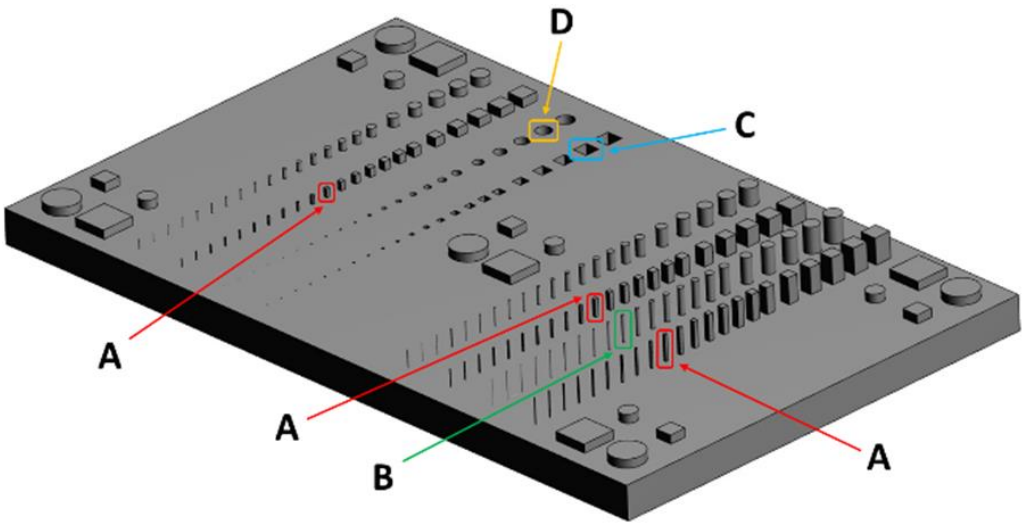

Fig 19: Benchmark artifact with microfeatures made by DLP-SLA [18]

The experiment proved that the main process parameters and the feature position in the build platform influenced the minimum achievable feature size. Also, it showed that the positive features were fabricated properly but the further investigation needs to be carried out for the negative features.

1.6 OBJECTIVES

The main objective of the thesis is to design a benchmark artifact, consisting of simple and complex geometry with various cross-sections, for the investigation of lab-on-chip manufacturing by digital light processing stereolithography process. The geometries and cross-sections could include simple geometrical features(such as extrusions, intrusions, holes etc) as well as complex ones like that of planar and nonplanar 3D-channels with various geometries (such as straight, serpentine, helical etc)and cross-sections (such as square, rectangular, circle etc) along with various junctions (such as T and Y) to evaluate the Digital Light Processing Stereolithography process. To design the benchmark artifact, several channel sections, and designs of literature reviews on the benchmark artifacts along with typical features of microfluidic devices are to be studied carefully. Apart from this, the results of a preliminary experimental campaign performed on the artifact, which is established in a bachelor thesis "Studio preliminare della fattibilità dell'ultra-fast prototyping di Lab-on-a-Chip mediante stereolitografia", thus enabling the establishment of new benchmark artifact. By considering this study as a reference, future in-depth research can be made using much more complex features, channels, and junctions.

CHAPTER 2: PRELIMINARY EXPERIMENTAL CAMPAIGN

2. PRELIMINARY EXPERIMENTAL CAMPAIGN

The design of the benchmark artifact proposed in this study is based on the literature review (Chapter 1) and the findings of a preliminary experimental campaign, which is being done on a benchmark artifact proposed in the bachelor thesis “Studio preliminare della fattibilità dell’ultra-fast prototyping di Lab-on-Chips mediante stereolitografia”.

This chapter deals with an existing benchmark artifact which is simple in its design layout, the experimental set-up, and the qualitative as well as the ANOVA analysis performed on the experimental campaign results of the simple features such as square intrusions, square extrusions, round intrusions and round extrusions. The features on the existing benchmark artifact were fabricated by varying the process parameters such as layer thickness and exposure time.

2.1 EXISTING BENCHMARK ARTIFACT WITH SIMPLE FEATURES

Fig.20 depicts the benchmark artifact that was proposed in the bachelor thesis “Studio preliminare della fattibilità dell’ultra-fast prototyping di Lab-on-Chips mediante stereolitografia”. Based on the size of the machine-building platform, the dimensions of the artifact base plate (width x height x thickness) was 45 × 28 × 2.5 mm.

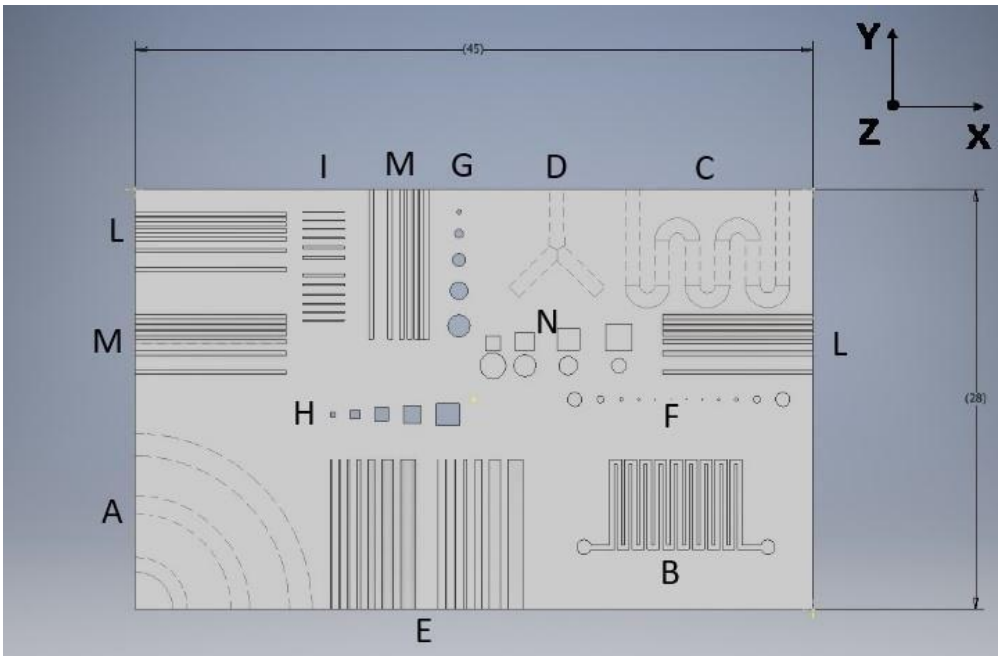

Figure 17 : Artifact layout [38].

As depicted in the Fig 19, the artifact includes:

- simple “positive” features, protruding above the base plate with a maximum height of 0.5 mm, (F+, I+ and N series).
- simple “negative” features, expanding below the base plate (E, F-, G, H, I-, L and M series).
- more complex features resembling typical channel geometries that can be found in microfluidic devices (A, B, C, and D).

The feature B and the features of the E, L, and M series are open channels.

It should be noted that the negative features and channels have their axis lying both in a plane perpendicular and parallel to the machine-building platform.

Feature	**Cross-section shape**	**Dimensions**
A	round	section diameter = 1, 1.25, 1.5 mm
B	square	section width = 0.3 mm
C	round	section diameter = 1 mm
D	round	section diameter = 1 mm
E	semi round and square	section diameter/width = 0.03, 0.06, 0.12, 0.24, 0.48, 0.72, 0.96 mm
F+	round	section diameter = 0.03, 0.06, 0.12, 0.24, 0.48, 0.72, 0.96 mm
F-	round	section diameter = 0.03, 0.06, 0.12, 0.24, 0.48, 0.72, 0.96 mm depth = 0.5 mm
G	round	section diameter = 0.3, 0.6, 0.9, 1.2, 1.5 mm
H	square	section width = 0.3, 0.6, 0.9, 1.2, 1.5 mm
I+	rectangular	thickness = 0.03, 0.06, 0.09, 0.12, 0.15, 0.18 mm
I-	rectangular	thickness = 0.03, 0.06, 0.09, 0.12, 0.15, 0.18 mm depth = 0.5 mm
L	semi round and square	section diameter/width = 0.3 mm distance = 0.03, 0.06, 0.12, 0.24, 0.48, 0.96 mm

M	semi round and square	section diameter/width = 0.3 mm distance = 0.03, 0.06, 0.12, 0.24, 0.48, 0.96 mm
N	round and square	section diameter/width = 1, 1.25, 1.5, 1.75 mm distance = 0.125, 0.25, 0.375, 0.5 mm height = 0.5 mm

Table 1: Cross-section shape and dimensions of benchmark artifact features

2.2 EXPERIMENTAL SETUP

The machine utilised to fabricate the benchmark specimen is Envision TEC Micro Plus HD [26] (Fig. 21), which is a Digital Light Processing (DLP) Stereolithography machine, which has a building platform of 45 x 28 x 100 mm, an XY resolution of 30 μm and a minimum Z resolution equal to 25 μm.

Figure 18 EnvisionTEC Micro Plus HD [26]

Based on the potential applications of Lab-On-Chip (LOC) devices, the resin utilised to fabricate the artifact is the Envision TEC E-shell 300 [18, 26] water clear, which is a biocompatible transparent photocuring methacrylic/acrylic resin.

For the first rough cleaning, the specimen is removed from the base and immersed in a 96% ethyl alcohol solution for a few minutes. An ultrasonic bath is also used to remove all the excess resin. If in any case the internal channels are clogged, a syringe can be used for their clearing.

The microfeatures of all benchmark artifacts were acquired and measured using a Zeiss Stereo discovery V20 optical microscope.

2.3 EXPERIMENTAL DESIGN

FACTOR	LEVELS	VALUES
Layer thickness (μm)	3	50, 100, 150
Exposure time (ms)	3	7000, 9500, 12000

Table 2: Experimental design

Two replicates were performed for all the 9 experimental conditions, therefore the whole experimental design consisted of 18 completely randomized runs.

For the qualitative analysis, the channels of a quarter of the circle, (A in fig (19)); serpentine channels with square (B in fig (19)) and circular (C in fig (19)) cross-sections; Y channel (D in fig (19)) were to be studied to qualitative evaluate their presence under various values of layer thickness and exposure time.

For the ANOVA analysis, features such as extrusions (square (N in fig (19)) and round (N in fig (19))) and holes (square (H in fig (19)) and round (G in fig (19))) were studied. The ANOVA analysis is to be done to evaluate the significance of the layer thickness and exposure time on the spatial repeatability, in a quest of which the dimensional error was to be analysed. The dimensional error of a feature is the absolute value of the difference between the measured and the nominal value of that feature.

2.4 QUALITATIVE ANALYSIS

2.4.1 Circle quarter channels

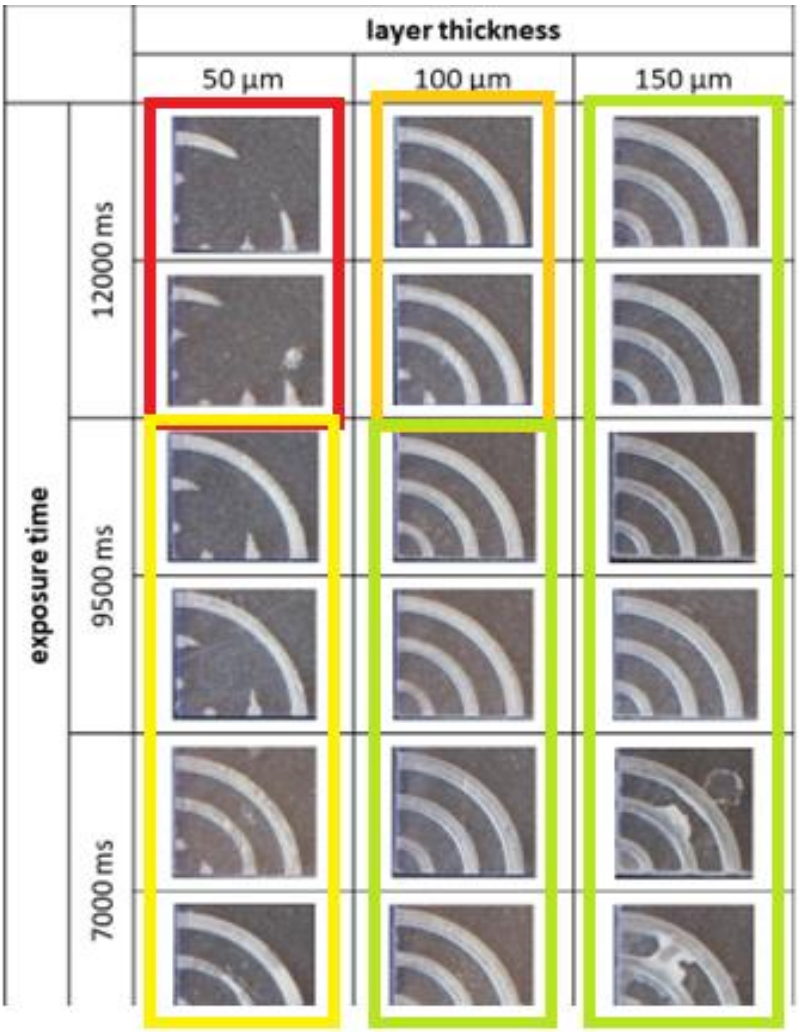

Figure 192 Comparison between the circle quarter channels [38].

Fig.22 depicts the circle quarter channels (A in Fig. 19) fabricated for each experimental condition. These channels are concentric and have diameters 1 mm, 1.25mm, and 1.5 mm respectively.

As depicted in they are three regions-red, orange, and green. The red region comprises of imperfectly formed channels, that is all the channels present were imperfectly formed. The orange region comprises of the partially formed channels, that is the channels with higher diameters were perfectly formed while the small diameter channels which were imperfectly

formed. The green region comprises of the channels that are perfectly formed, that is all the channels present were perfectly formed.

Thus, it can be observed that a low layer thickness (50 μm) and a high exposure time (12000 ms) lead to failure, that is channels are improperly formed.

The moderate layer thickness (100 μm) and high exposure time (12000 ms) result in partially formed channels, that is the inner channels with low diameters are improperly formed. The high layer thickness (150 μm) and high exposure time (12000 ms) result in forming acceptable quality product where all the channels are formed.

The low layer thickness (50 μm) and moderate exposure time (950 ms) lead to failure, that is channels are improperly formed. The moderate layer thickness (100 μm) and moderate exposure time (950 ms) result in forming acceptable quality product, where all the channels are formed. The high layer thickness (150 μm) and moderate exposure time (950 ms) also result in forming acceptable quality product, where all the channels are formed.

The low layer thickness (50 μm) and low exposure time (700 ms) lead to failure, that is improperly formed channels. The moderate layer thickness (100 μm) and low exposure time (700 ms) result in forming acceptable quality product where all the channels are formed. The high layer thickness (150 μm) and low exposure time (700 ms) result in over formed channels, wherein the channels are spread.

2.4.2 Serpentine channels with circular cross section

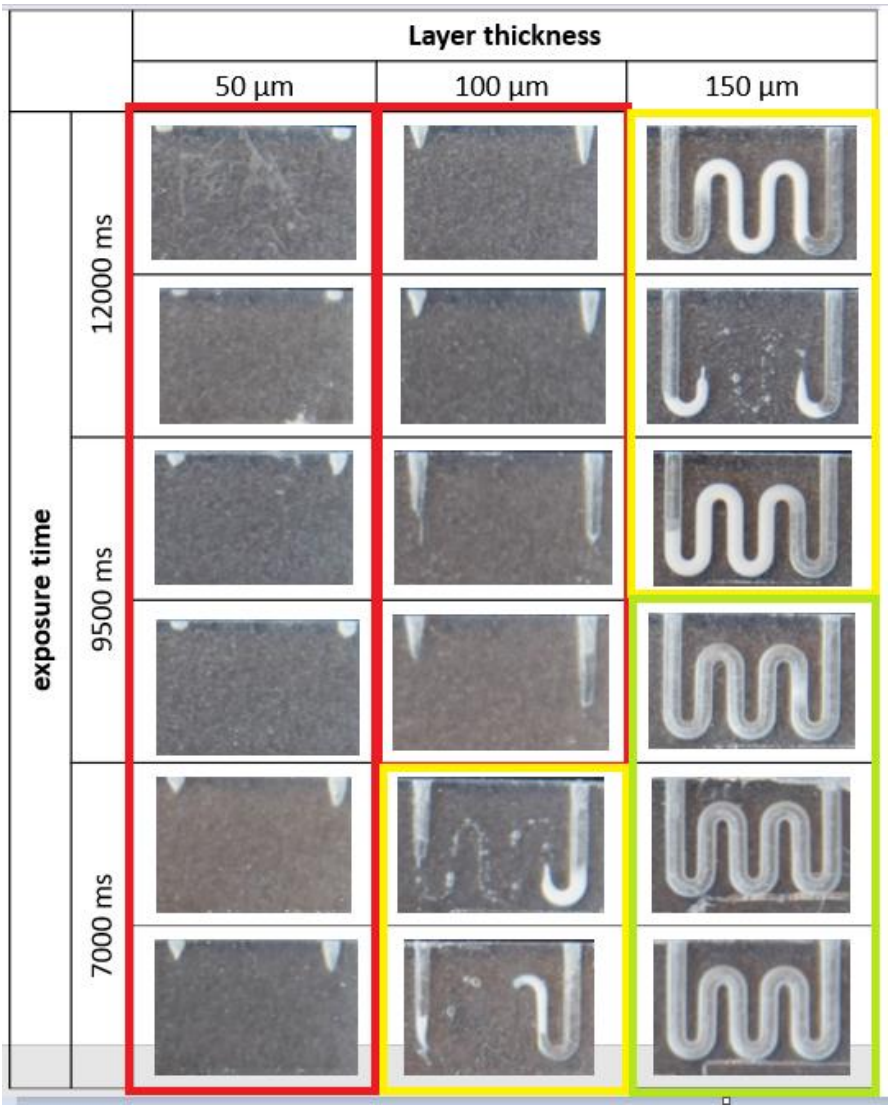

Figure 23 Comparison between the serpentine channels with circular cross section [38]

.

Fig 23 depicts the serpentine channels with circular cross section (C in Fig. 19) fabricated for each experimental condition.

As depicted in they are three regions-red, yellow, and green. The red region comprises of improperly formed channels, that is the channels could only be seen at the start and the end. The yellow region comprises of the blocked or partially formed channels, the green region comprises of the channels that are perfectly formed.

Thus, it can be observed that a low layer thickness (50 µm) and a high exposure time (12000 ms) lead to failure, that is channels are improperly formed. The low layer thickness (50 µm)

and moderate exposure time (950 ms) lead to failure, that is channels are improperly formed. The low layer thickness (50 μm) and low exposure time (700 ms) lead to failure, that is channels are improperly formed.

The moderate layer thickness (100 μm) and high exposure time (1200 ms) lead to failure, that is channels are improperly formed. The moderate layer thickness (100 μm) moderate exposure time (950 ms) lead to failure, that is channels are improperly formed. The moderate layer thickness (100 μm) and low exposure time (700 ms) lead in forming partially formed channels.

The high layer thickness (150 μm) and high exposure time (1200 ms) lead in forming partially formed channels. The high layer thickness (150 μm) and moderate exposure time (900 ms) lead in forming completely formed channels. The high layer thickness (150 μm) and low exposure time (700 ms) lead in forming perfect channels.

2.4.3 Y channel

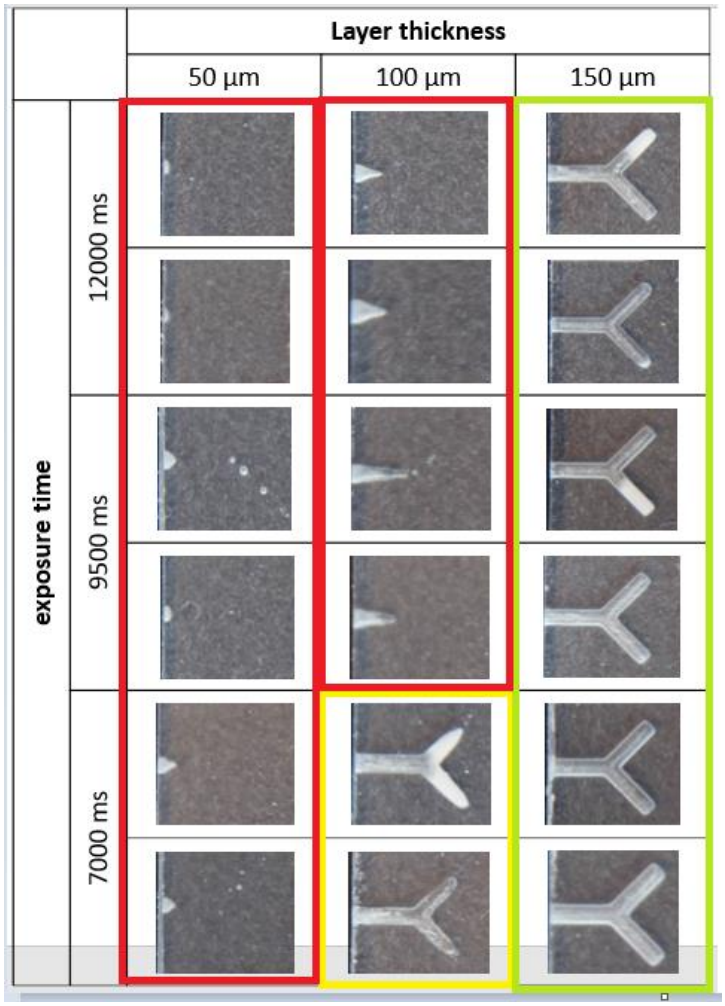

Figure 20 Comparison between the Y channels [38].

Fig. 24 depicts the Y channels (D in Fig. 19) fabricated for each experimental condition. The diameter of the channel cross-section is 0.5 mm. As depicted in they are three regions-red, yellow, and green.

The channels in the red region are not satisfactory except for the input. Partial channels are shown in yellow region, but the channels are not formed completely. Satisfactory results are shown in the channels that are present in the green region.

The only satisfactory channels are those obtained at high thicknesses layer (150 µm), while all other combinations of parameters did not form the channels properly. The combination (100 µm -7000 ms) provides partial satisfactory results although not leading to a complete Y channel shape.

2.4.4 Channels with square cross-section

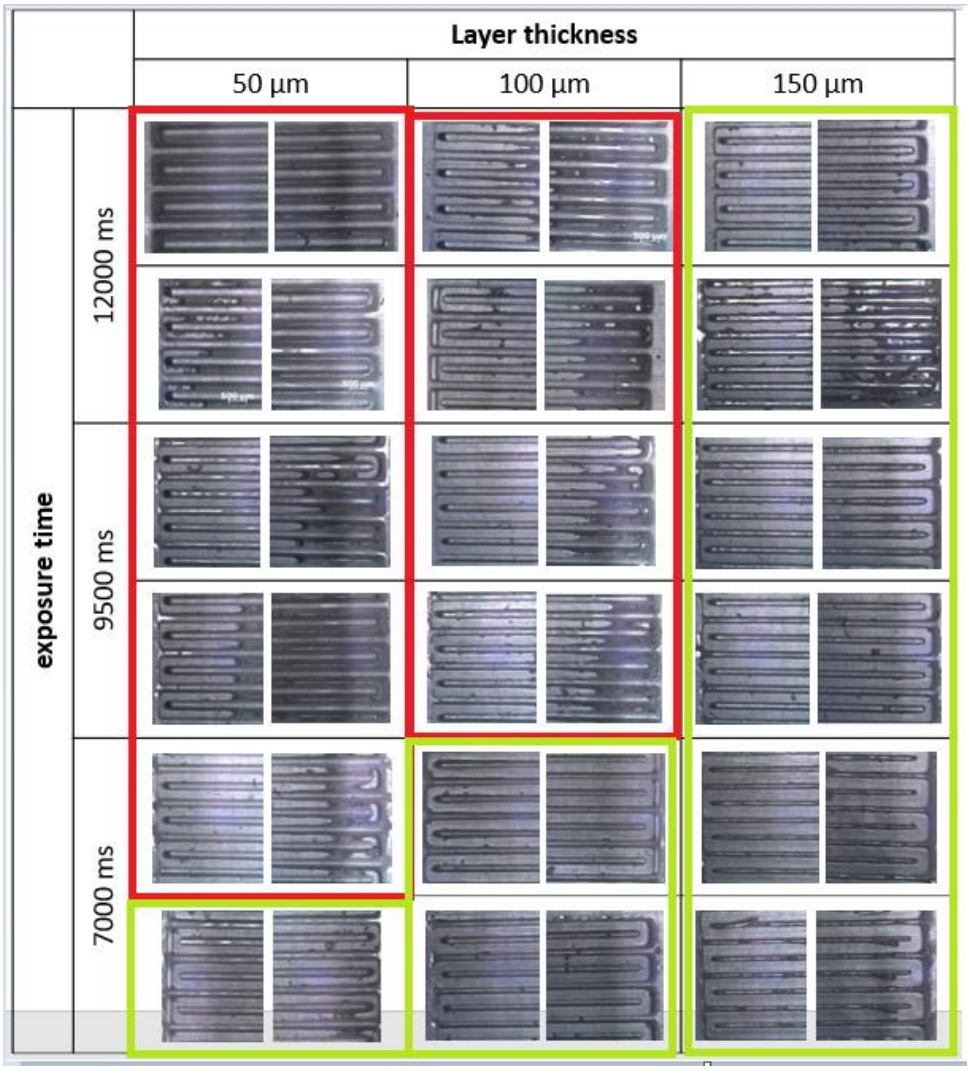

Figure 21 Comparison between the serpentine channels with square cross section [38].

Fig. 25 shows the pictures of the serpentine channels with square cross section (B in Fig. 19) fabricated for each experimental condition. The side of the square channel is 0.3mm. As depicted in they are three regions-red and green.

The channels present in red region are incomplete channels and the channels in green region are completely formed and show satisfactory results.

Thus, it can be observed that a low layer thickness (50 µm) and a high exposure time (12000 ms) lead to failure, that is channels are improperly formed. The low layer thickness (50 µm)

and moderate exposure time (950 ms) lead to failure, that is channels are improperly formed. The low layer thickness (50 μm) and low exposure time (700 ms) show satisfactory results, that is channels are properly formed.

The moderate layer thickness (100 μm) and high exposure time (1200 ms) lead to failure, that is channels are improperly formed. The moderate layer thickness (100 μm) moderate exposure time (950 ms) lead to failure, that is channels are improperly formed. The moderate layer thickness (100 μm) and low exposure time (700 ms) show satisfactory results, that is channels are properly formed.

The high layer thickness (150 μm) and high exposure time (1200 ms) show satisfactory results, that is channels are properly formed with certain imperfections owing to the resin accumulation. The high layer thickness (150 μm) and moderate exposure time (900 ms) show satisfactory results, that is channels are properly formed. The high layer thickness (150 μm) and low exposure time (700 ms) show satisfactory results, that is channels are properly formed with some walls being detached.

2.4.5 Comments on qualitative analysis results

The general performance of the ratings shows a failure rate for the tests made with a thickness of layer 50 μm, along with high exposure time of 1200 ms. while the choice of high layer thickness (150 μm) along with moderate (950 ms) to low exposure times (700 ms) has proved more effective.

The Digital light Processing Stereolithography (DLP-SLA) involves fabrication of product using layer by layer mechanism, where the resin is being cured by the digital light projector. During the fabrication of the internal features of a thin thickness at high exposure time, the resin will block the canals or sometimes will lead to the accumulation of the resin. While the channels and features with high layer thickness combined with moderate to low exposure times show satisfactory results.

2.5 ANOVA ANALYSIS

2.5.1 Negative feature with circular section

A feature from G series with diameter 1.5 mm was fabricated using digital light processing stereolithography (DLP-SLA) process, with variations in layer thicknesses and exposure times. The experimental results related to the dimensional error are shown in Fig. 26B (for the sake of brevity, the values are listed in table 7 of the appendix) while the ANOVA results are reported in Table 3.

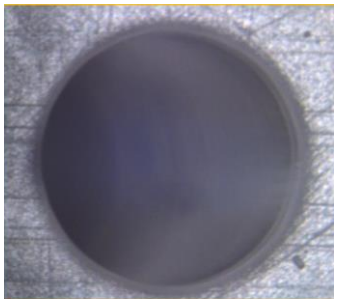

Figure 226A an example of G feature with diameter = 1.5 mm [38].

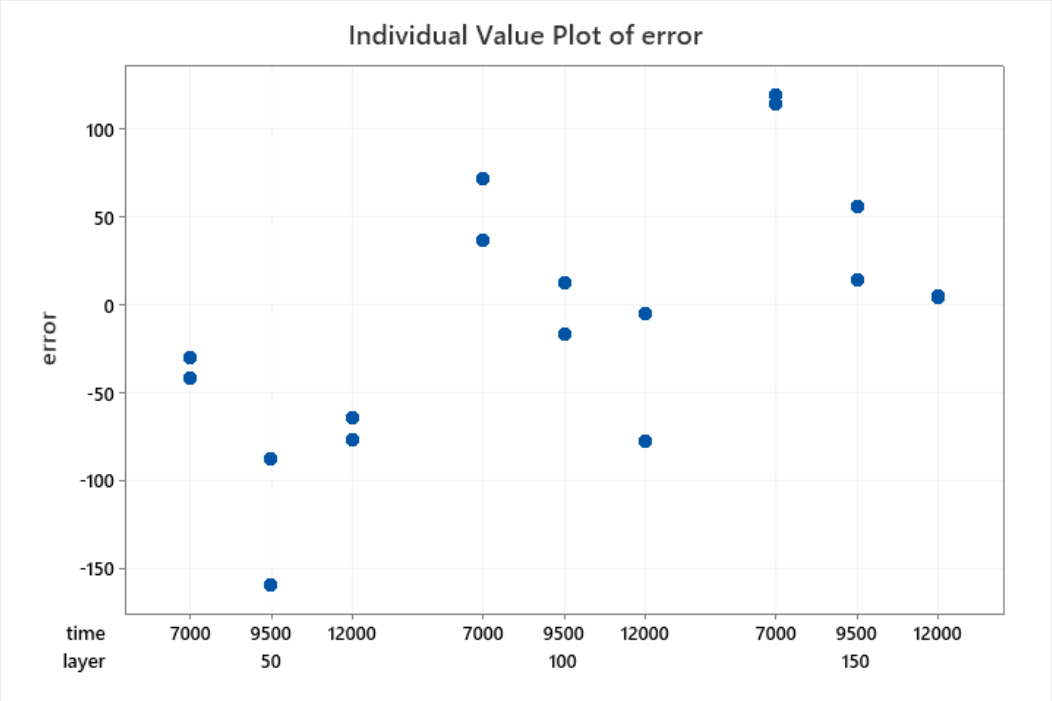

Figure 23B Individual value plot of the dimensional error of G feature with diameter = 1.5 mm

Table 3: ANOVA p-values (green = significant factor, confidence level α = 5 %) for the analysis on the dimensional error of G feature with diameter = 1.5 mm

Source	DF	Adj SS	Adj MS	F-Value	P-Value
Model	8	81007	10125.9	12.51	0.000
Linear	4	74987	18746.8	23.16	0.000
layer	2	50589	25294.3	31.25	0.000
time	2	24399	12199.4	15.07	0.001
2-Way Interactions	4	6020	1504.9	1.86	0.202
layer*time	4	6020	1504.9	1.86	0.202
Error	9	7285	809.4		
Total	17	88292			

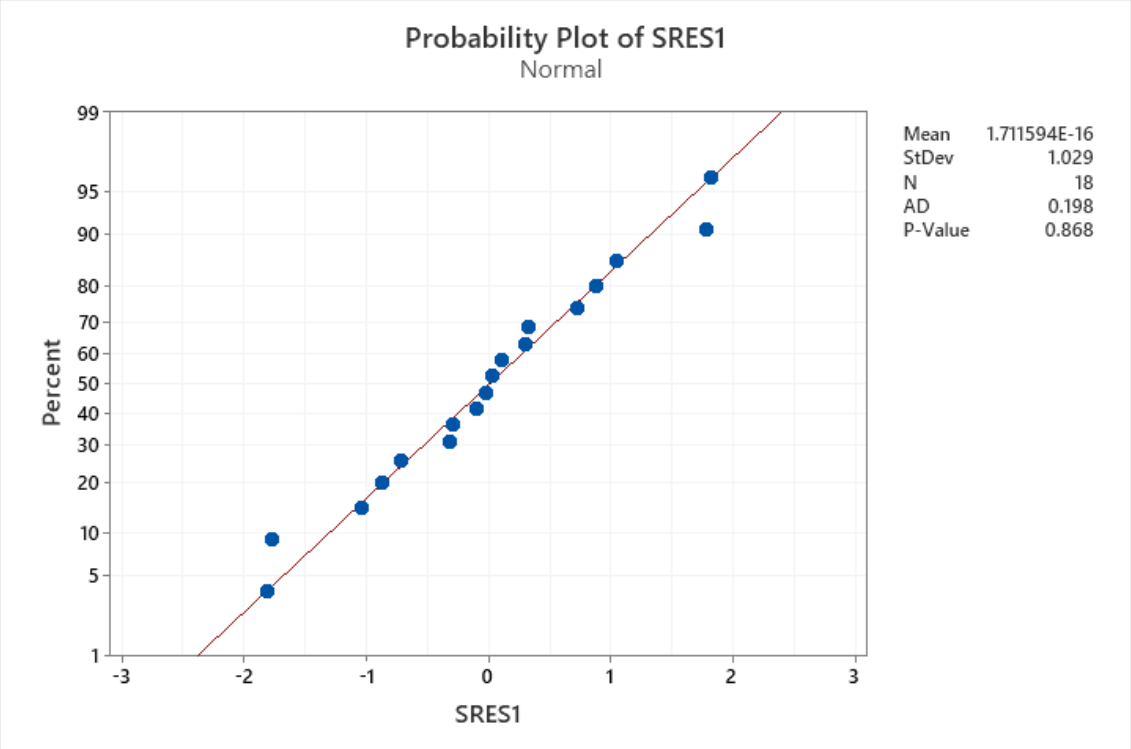

Figure 24 Probability plot of standardized residuals for the ANOVA on the dimensional error of G feature with diameter = 1.5 mm

The analysed model fully satisfied the ANOVA hypotheses of normality (Anderson-Darling p-value = 0.868), equal variances and time independence of residuals. Moreover, its coefficient of determination R^2_{adj} is equal to 84.42% and demonstrate the model adequacy to explain the observed data variability. ANOVA results (Table 3) show that the feature dimensions are influenced by the layer thickness, the exposure time, and their interaction, thereby indicating them to be significant factors.

2.5.2 Negative feature with square section

Feature from H series with width 1.5 mm was fabricated using DLP-SLA process, with variations in layer thicknesses and exposure times. The experimental results related to the dimensional error are shown in Fig. 29 (for the sake of brevity, the values are listed in Tab. 8 in the appendix) while the ANOVA results are reported in Table 4.

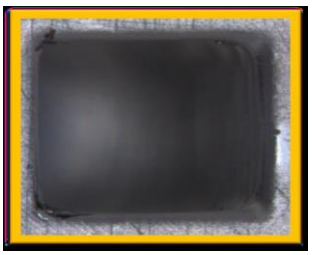

Figure 25 Example of square with Intrusion and side 1.5 mm [38].

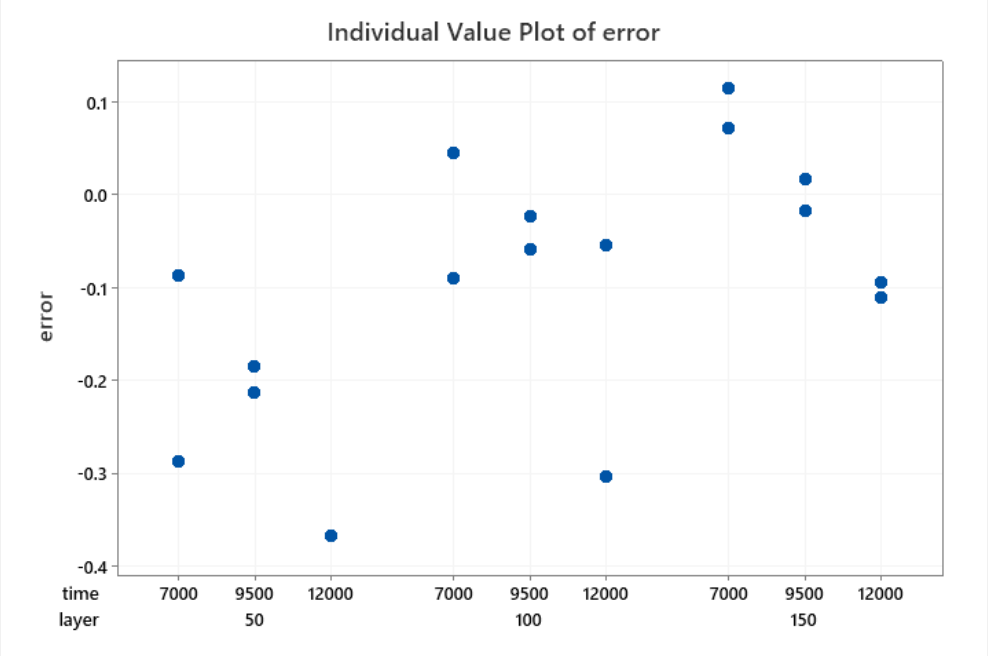

Figure 26 Individual value plot of the dimensional error of H feature with width = 1.5 mm.

Table 4: ANOVA p-values (green = significant factor, confidence level α = 5 %) for the analysis on the dimensional error of H feature with width = 1.5 mm

Source	DF	Adj SS	Adj MS	F-Value	P-Value
Model	8	0.231997	0.029000	3.69	0.041
Linear	4	0.213865	0.053466	6.81	0.011
layer	2	0.161052	0.080526	10.25	0.006
time	2	0.085497	0.042748	5.44	0.032
2-Way Interactions	4	0.004572	0.001143	0.15	0.960
layer*time	4	0.004572	0.001143	0.15	0.960
Error	8	0.062829	0.007854		
Total	16	0.294826			

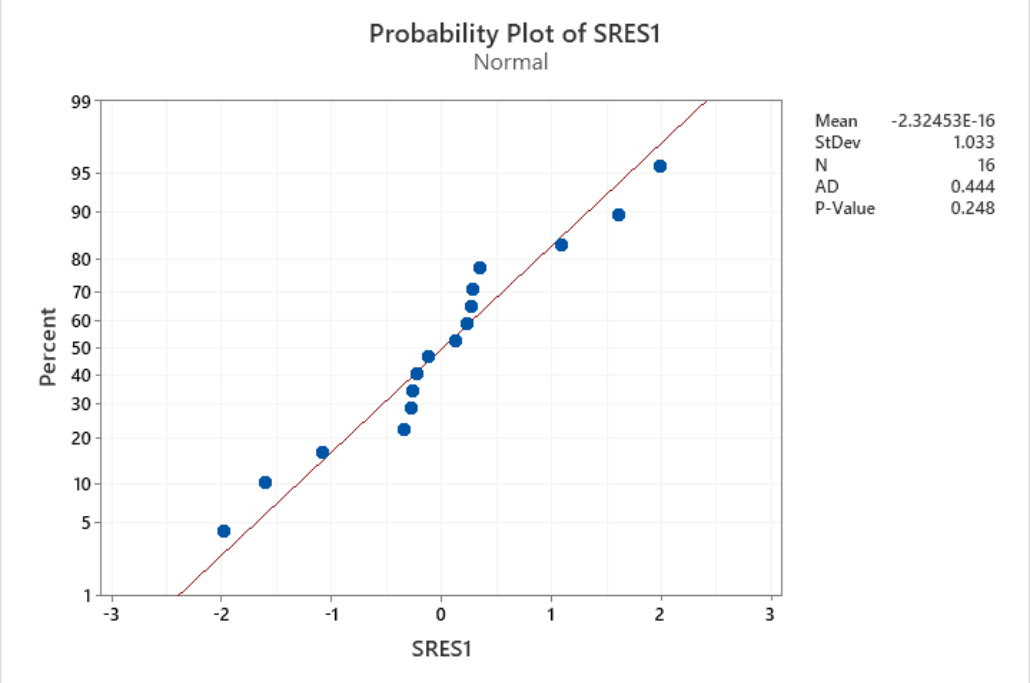

Figure 27 Probability plot of standardized residuals for the ANOVA on the dimensional error of H feature with width = 1.5 mm

The analysed model fully satisfied the ANOVA hypotheses of normality (Anderson-Darling p-value = 0.248), equal variances and time independence of residuals. Moreover, its coefficient of determination R^2_{adj} is equal to 57.38% and demonstrate the model adequacy to explain the observed data variability.

ANOVA results (Table 4) show that the feature dimensions are influenced by the layer thickness, the exposure time, and their interaction, thereby indicating them to be significant factors.

2.5.3 Positive feature with circular section

N round feature with diameter = 1.25 mm was fabricated using DLP-SLA process, with variations in layer thicknesses and exposure times. The experimental results related to the dimensional error are shown in Fig. 32 (for the sake of brevity, the values are listed in Tab. 9 in the appendix) while the ANOVA results are reported in Table 5.

Figure 28 Extruded features with round section [2].

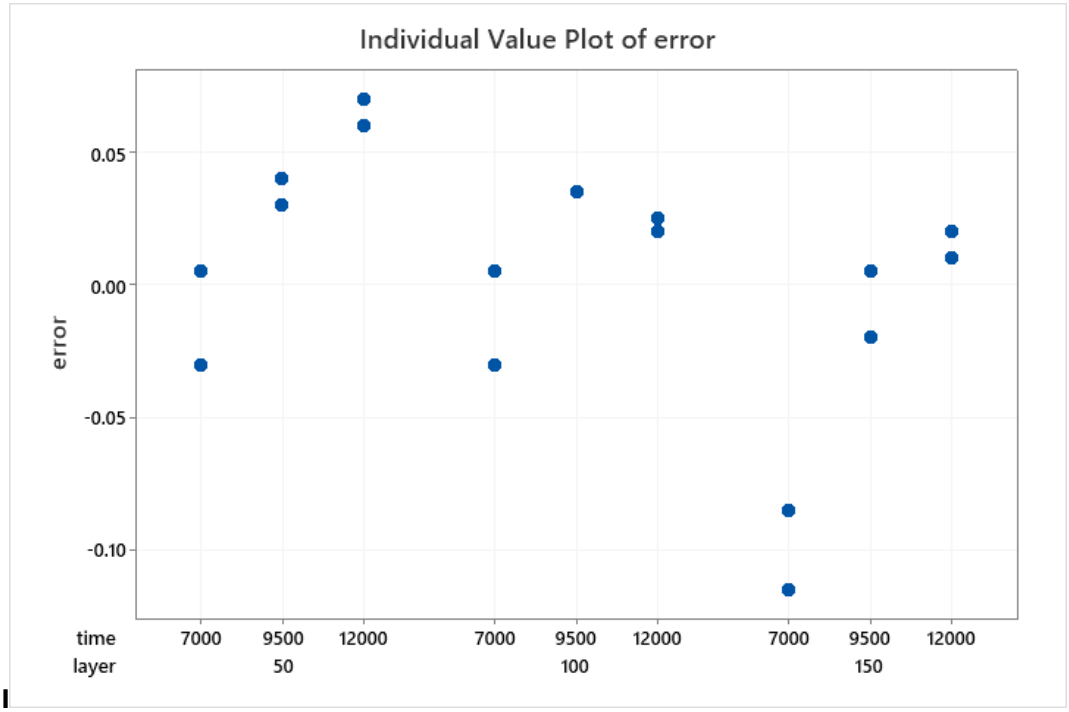

Figure 29 Individual value plot the dimensional error of N round feature with diameter = 1.25 mm.

Table 5: ANOVA p-values (green = significant factor, confidence level α =5 %) for the analysis on the dimensional error of N round feature with diameter = 1.5 mm

Source	DF	Adj SS	Adj MS	F-Value	P-Value
Model	8	0.034206	0.004276	15.91	0.000
Linear	4	0.030467	0.007617	28.34	0.000
layer	2	0.011620	0.005810	21.62	0.001
time	2	0.019230	0.009615	35.78	0.000
2-Way Interactions	4	0.003704	0.000926	3.45	0.064
layer*time	4	0.003704	0.000926	3.45	0.064
Error	8	0.002150	0.000269		
Total	16	0.036356			

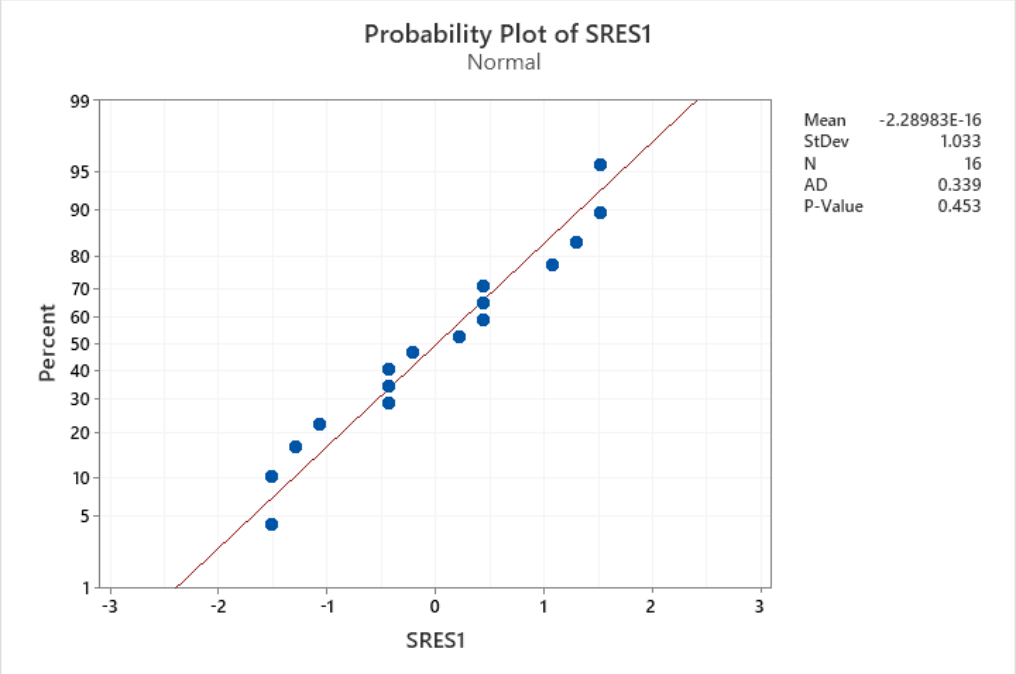

Figure 30 Probability plot of standardized residuals for the ANOVA on the dimensional error of N round feature with diameter = 1.5 mm

The analysed model fully satisfied the ANOVA hypotheses of normality (Anderson-Darling p-value = 0.453), equal variances and time independence of residuals. Moreover, its coefficient of determination R^2_{adj} is equal to 88.17% and demonstrate the model adequacy to explain the observed data variability.

ANOVA results (Table 4) show that the feature dimensions are influenced by the layer thickness, the exposure time, and their interaction, thereby indicating them to be significant factors.

2.5.4 Positive feature with square section

N square feature with diameter = 1.25 mm was fabricated using DLP-SLA process, with variations in layer thicknesses and exposure times. The experimental results related to the dimensional error are shown in Fig. 35 (for the sake of brevity, the values are listed in Tab. 10 in the appendix) while the ANOVA results are reported in Tab. 6.

Figure 31 extrusion feature with square section [2].

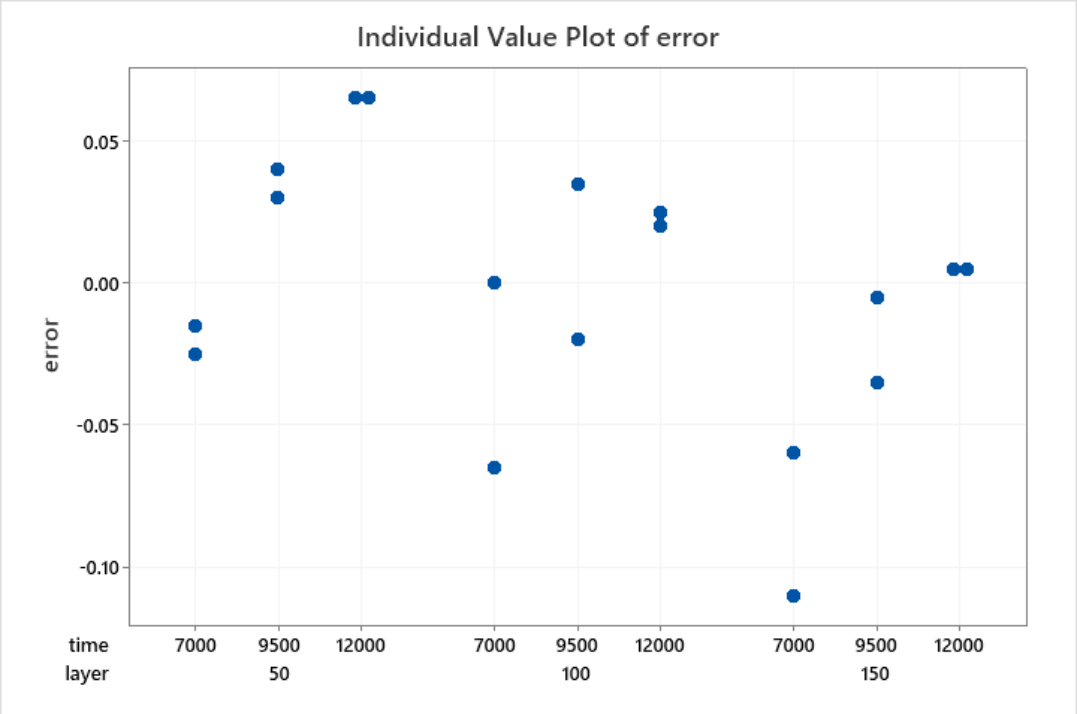

Figure 32 Individual Value Plot of the dimensional error of N square feature with width = 1.5 mm.

Table 6: ANOVA p-values (green = significant factor, confidence level α =5 %) for the analysis on the dimensional error of N square feature with width = 1.5 mm

Source	DF	Seq SS	Contribution	Adj SS	Adj MS	F-Value	P-Value
Model	8	0.030125	84.71%	0.030125	0.003766	6.23	0.006
Linear	4	0.029358	82.55%	0.029358	0.007340	12.15	0.001
layer	2	0.010825	30.44%	0.010825	0.005413	8.96	0.007
time	2	0.018533	52.11%	0.018533	0.009267	15.34	0.001
2-Way Interactions	4	0.000767	2.16%	0.000767	0.000192	0.32	0.860
layer*time	4	0.000767	2.16%	0.000767	0.000192	0.32	0.860
Error	9	0.005438	15.29%	0.005438	0.000604		
Total	17	0.035563	100.00%				

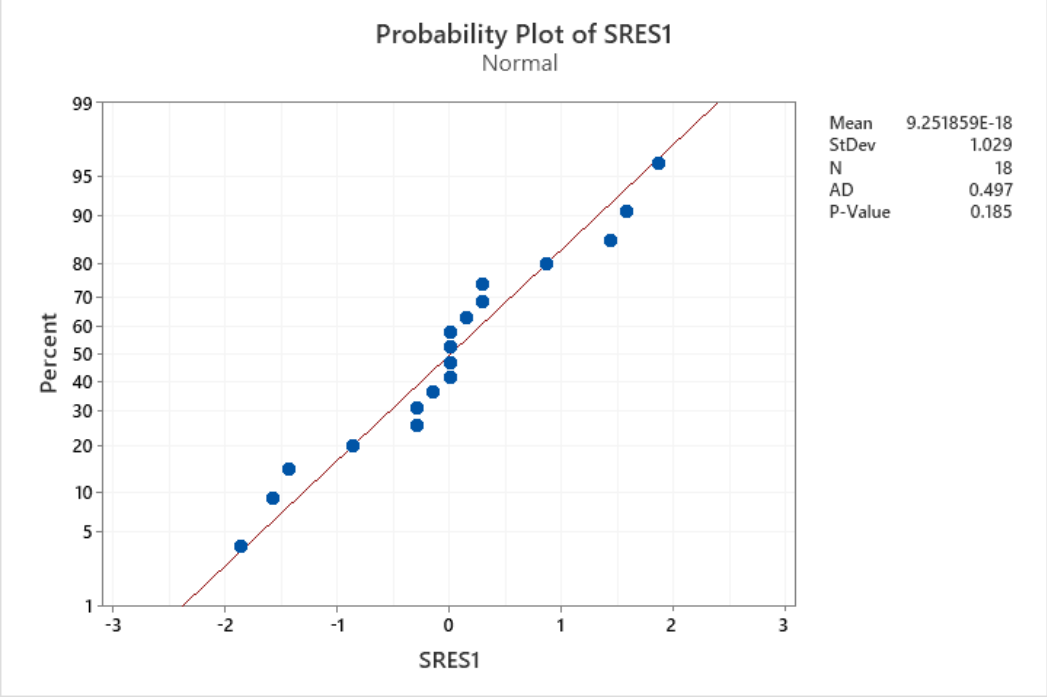

Figure 33 Probability plot of standardized residuals for the ANOVA on the dimensional error of N square feature with width = 1.5 mm

The analysed model fully satisfied the ANOVA hypotheses of normality (Anderson-Darling p-value = 0.453), equal variances and time independence of residuals. Moreover, its coefficient of determination R^2_{adj} is equal to 71.12% and demonstrate the model adequacy to explain the observed data variability.

ANOVA results (Table 6) show that the feature dimensions are influenced by the layer thickness, the exposure time, and their interaction, thereby indicating them to be significant factors.

2.5.5 Comments on ANOVA analysis results

The above specified tables and figures (from Fig 26 to 34 & Table 3 to 6) depicted the following results-

The ANOVA hypotheses of normality, equal variances and time independence of residuals was fully satisfied by models that were being analysed. The layer thickness and the exposure time affected dimensional accuracy and quality of the feature, thus indicating them to be significant factors.

For positive features, the dimensional error increases with an increase in exposure time and/or with the decrease in layer thickness. The error is a result of UV curing either from a deficient resin curing to the curing of larger unwanted regions .For the negative features, the deficient resin curing at low exposure time values and/or at high layer thickness values result in bigger feature size and vice versa.

Thus, it is evident that low exposure time and high layer thickness results in obtaining the desired quality product(channels).

The square section has the values of dimensional error greater than those regarding the features with a round section owing to the accumulation of an excess resin at the vertices for a feature with square section.

.

CHAPTER 3

PROPOSED BENCHMARK ARTIFACT DESIGN

3. PROPOSED BENCHMARK ARTIFACT DESIGN

The existing studies that are discussed earlier in the Literature review (Chapter 1) and the preliminary experimental campaign (Chapter 2) laid a foundation for the proposed benchmark artifact. The artifacts discussed included several simple and complex geometries which had planar and nonplanar channels, 3D helical channel, extrusion/intrusions, etc. These features are required to evaluate the geometrical performance of the digital light processing (DLP) Stereolithography machine for manufacturing the Complex microfluidic features.

3.1 DIMENSIONING THE BENCHMARK ARTIFACT

The general dimensions of the building platform are 45 × 28 × 100 mm [18]. Thus, the dimensions of the proposed benchmark artifact considered are 45 × 28 mm so that the artifact could cover all the build platform. The thickness chosen is 2.5 mm (Fig 37)

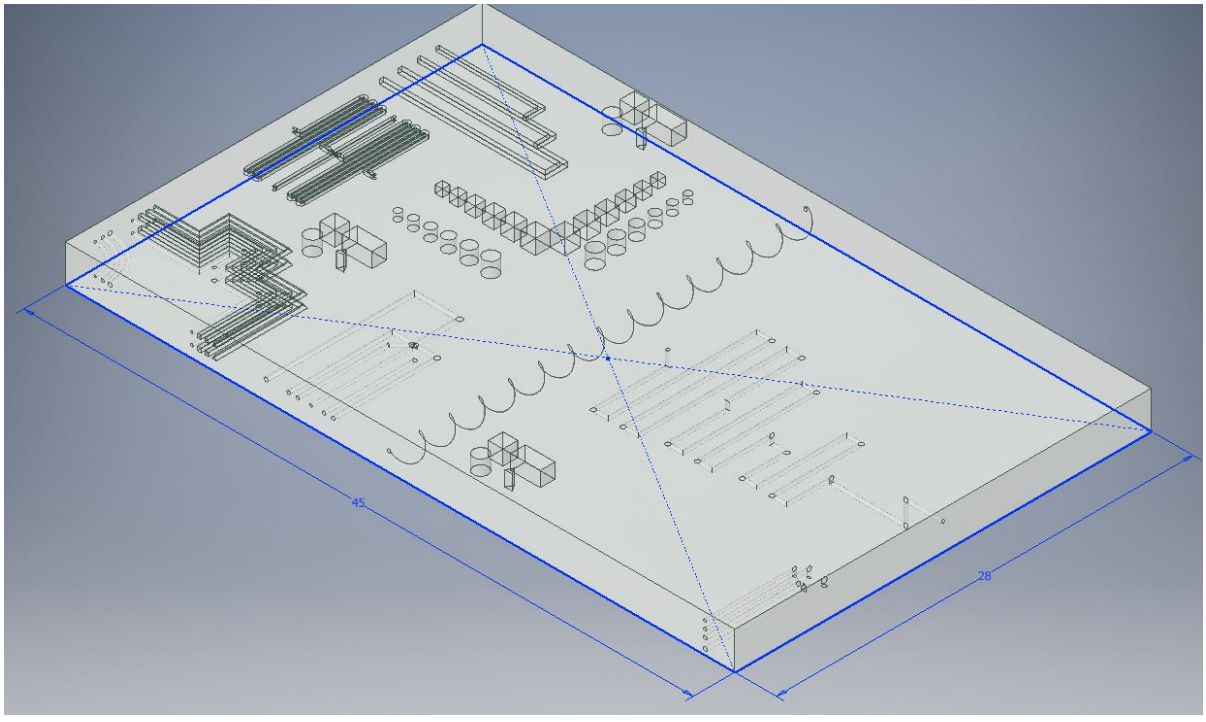

Figure 34 Benchmark artifact with dimensions 45 × 28 × 2.5mm3

The entire specimen is divided into two halves: one half has planar channels with different features, geometry, and cross-section and the other half consists of non-planar channels (Fig 38).

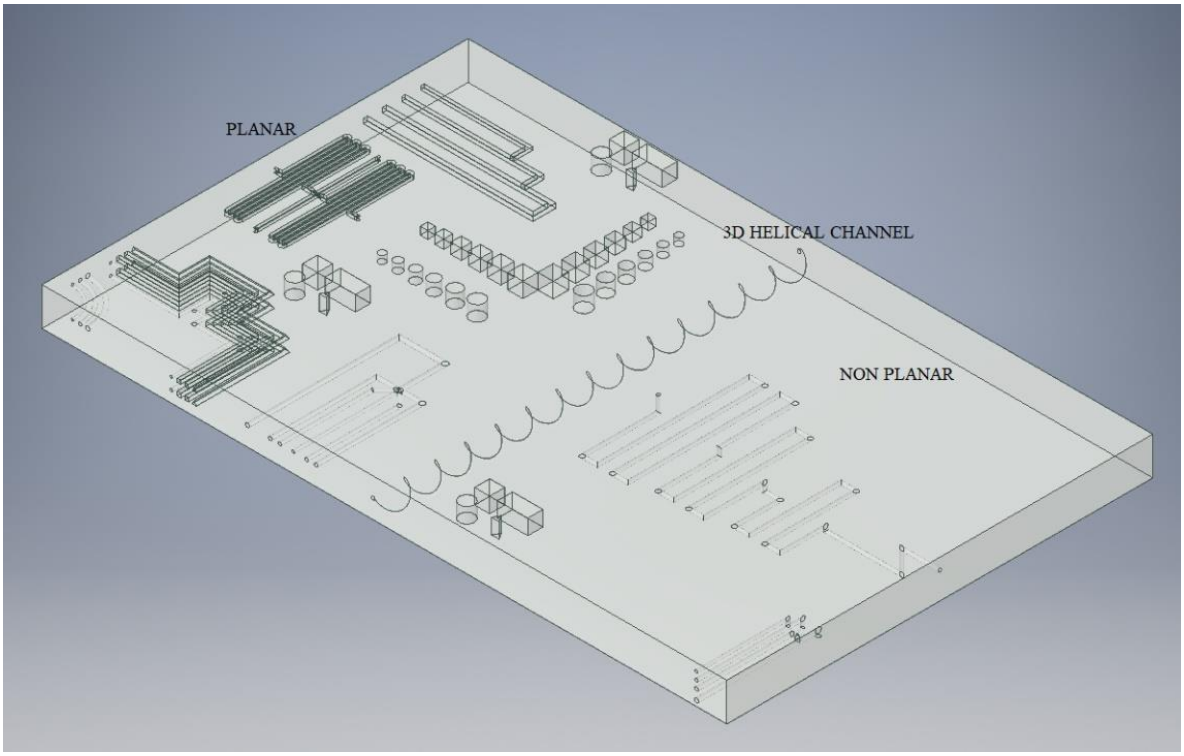

Figure 35 representation of planar and non-planar channels in the chip

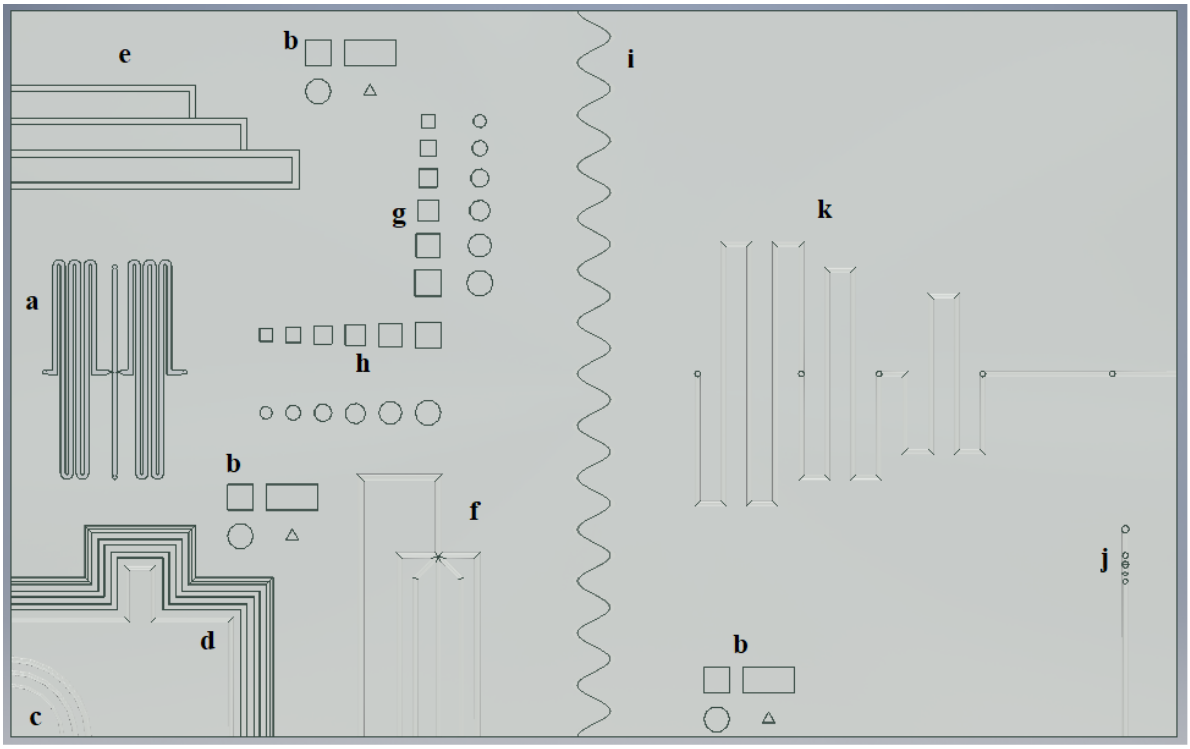

Figure 36 representation of all the features in the chip

A detailed list of all the features, shapes, dimensions, and the reason for choosing these features is mentioned below individually. Considering the results from the literature (Section 1.5.1) and the preliminary experimental campaign (Chapter 2), and keeping in mind that the XY resolution of 30 μm and a minimum Z resolution equal to 25 μm for the selected DLP machine [18] the dimension of the channels and the size are chosen. The reason for choosing all the below features is that these are mostly used in the manufacturing of the microfluidic devices. The features are opted depending on the application, for example, for emulsion formation, mainly straight channels with T and Y junction are chosen. For drug delivery and cell detection curved channels with varying cross section and size are chosen. Also, existing studies [18, 38] shows that the planar channels can be manufactured using the present DLP machine. The manufacturability of the nonplanar channels needed to be investigated. All these features have benefits of their own.

3.1.1 Planar:

a) Extrusions design

b) Spatial repeatability geometry with a set of square, circle, triangle, and rectangle.

c) Curved channels inside the chip (circular cross-section with different sizes)

d) Channels with different geometry and different sizes (circular, rectangle, square, and triangle) inside the chip.

e) T junction inside the chip (Rectangular cross-section with different sizes)

f) Y- Junction inside the chip (circular cross-section with different sizes)

g) Intrusion for square and circle (different sizes)

h) Extrusion for square and circle (different sizes)

3.1.2 Non-Planar:

i) A helical channel at midway length

j) Non-planar circular channel with T and Y junction inside by varying size.

k) Complex 3-dimensional nonplanar channel

Feature dimensions are:

Extrusions design: This type of design (Fig 40) is widely used in most microfluidic chip fabrication field for the detection of the cancer cells separation in the blood samples. It is a straight and serpentine channel combination which are inspired from the microfluidics shown fig (8), fig (9) & fig (10). They are easy to fabricate and have an ability for parallelization. However, the flow within a straight microchannel is a function of its cross-section. Generally, when the width to height ratio becomes high, stable focusing channels are reduced. flow cytometry applications are mainly exploited, with the usage of the straight microchannels [26].

Sinusoidal or serpentine microchannels have a better focusing performance, the ability of massive parallelization, with a small footprint. This better focusing performance is owing to the curvature direction changes in each loop, thus making them qualify for applications, involving a high-throughput separation for micron and sub-micron bioparticles (cyanobacteria) and harvesting of cyanobacteria [26].

By altering the design from curvilinear to straight, a sinusoidal microchannel with a square-wave pattern is obtained which enables a size-based particle focusing with unique features.

a) This design has three inlets (one left, one top, and one at the bottom) and the outlet is at the right end. This design was opted to check the positive features manufacturability also to check the flow of three similar/dissimilar fluids from the three inlets, mixing in the centre and the result of the mixer is collected in the outlet. Serpentine channels are wide part of microfluidic devices, they have a better focusing performance, the ability of massive parallelization, with a small footprint. It was included in the proposed benchmark with following dimensions.

Dimensions: Channels are of width 300 μm, depth 500 μm, and length 8.5 mm, the inlet, and outlet diameters are 180 μm.

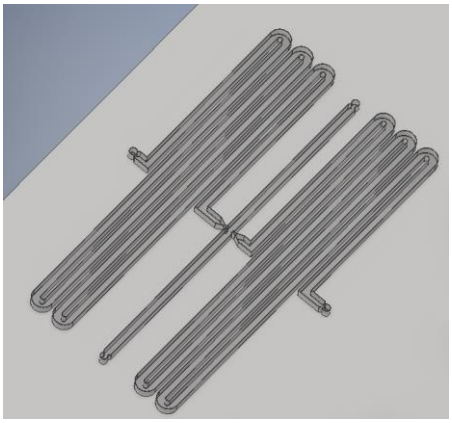

Figure 37 Extrusions design

b) Spatial repeatability geometry with a set of square, circle, triangle, and rectangle (Fig 41): These are the basic set of geometry to evaluate the system spatial repeatability at different locations on the benchmark, which is inspired from pre-existing benchmarks as shown in the fig(14A) and fig (14B). The sets are not close to each other but are far from each other for the better evaluation. Dimensions are 3 sets of identical positive features (Square 1 × 1 mm; Rectangle 2 × 1 mm; Triangle 0.5 mm and circle 1 mm diameter) and extruded height 1 mm.

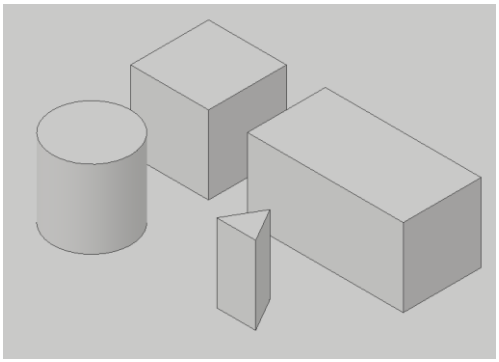

Figure 38 spatial repeatability set

c) Curved channels inside the chip (Fig 42): These are non-rectangular circular channels mostly used for fluid delivery in medical applications. It is inspired from the non-rectangular channels shown in fig (13).The fig 42 consists of curved channels with varying diameter 1 mm, 1.25 mm, and 1.5 mm, and the gap between each channel is 0.5 mm, gradually increasing according to the resolution of the DLP machine. The channels are placed at the corner of the chip so that the fluid enters from the inlet and leaves the chip at the outlet.

Figure 39 Curved channels inside the chip

d) Channels with different geometry and sizes inside the chip (Fig 43): They are used in microfluidics for formation of the emulsions, in drug delivery, cosmetics and to evaluate the internal fluid flow. They improve the fluid mixing in devices, operating at low Reynolds numbers (Re). They are mainly inspired from the microfluidics shown in the fig (10) and fig (13). These channels are widely used in the microfluidics, the channels are not straight but are bent at right angles to check how the flow rate will be in different cross sections. The inlets and outlets are placed at the corners, so the fluid exits freely.

   Here (fig 43) shows two sets of four different channels circular, rectangle, square, and triangle to evaluate the internal fluid flow in different cross-section and by varying their size. Circular channels with 1 mm and 1.25 mm; rectangular channels with 300 μm × 500 μm and 600 μm × 500 μm; square channels with 300 μm × 300 μm and 600 μm × 600 μm; equilateral triangular channels with 300 μm and 600 μm dimensions.

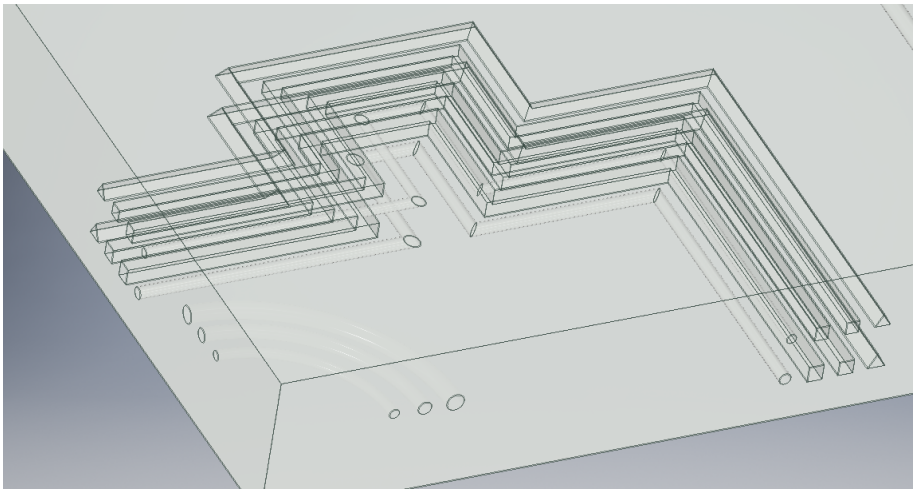

Figure 40 Channels with different geometry and sizes

e) T junction (Fig 44): To evaluate the formation of emulsions, rectangular channels with varying cross-section. Three inlets meet at the T junction and forms emulsion. Both the inlet and outlet are at the same side so that the fluid enters and leaves freely. This designed is inspired from the microfluidic device comprising of T-junction shown in fig (11). Different types of fluids can be injected through the inlets.

   Width × height dimensions are 300 μm × 500 μm, 600 μm × 500 μm, and 900 μm × 500 μm of top, middle, and down channels, respectively.

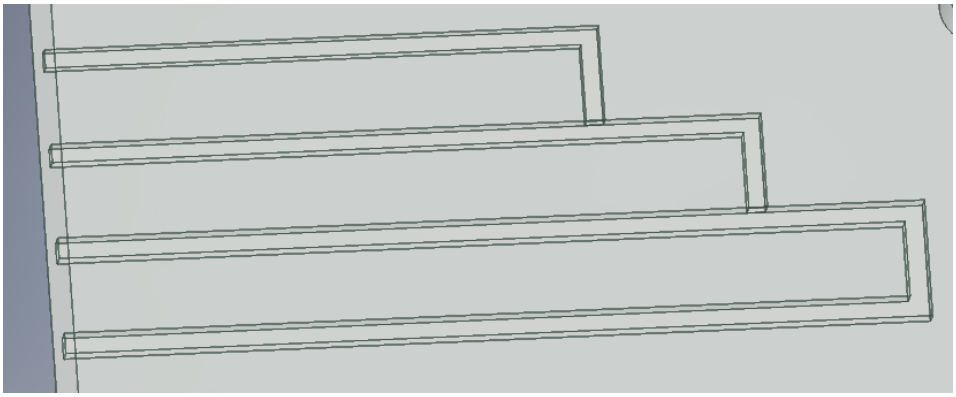

Figure 41 T junction rectangular channels

f) Y Junction (Fig 45): Three circular channel inlets and one outlet with gradual increment in diameter 1, 1.25, 1.5 and 1.75 mm. Both the T and Y junctions are used in the formation of the emulsions and cosmetics. Both the inlet and outlet are at the same side so that the fluid enters and leaves freely. This design of Y-junction is inspired from microfluidics shown in figure (12).

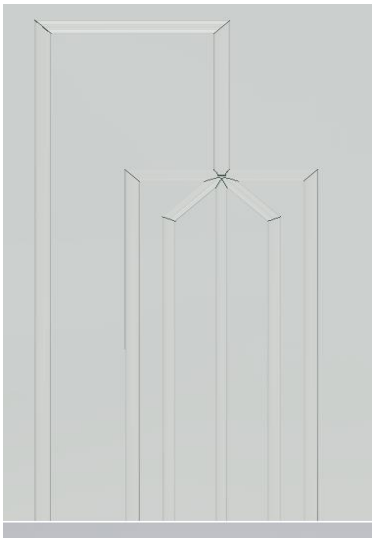

Figure 42 Y junction circular channels

g) Extrusion features square and circular geometry to evaluate the resolution of the selected DLP system. This designed is inspired from the pre-existing benchmarks shown in fig(14) and fig (15).Extrusion dimensions are square ranging from 0.5 mm to 1 mm in length/width/height and circle ranging from 0.5 mm to 1 mm in diameter/height (Fig 46).

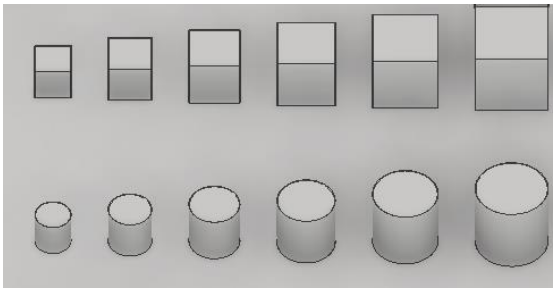

Figure 43 Extrusion geometry (square and circle)

h) Intrusion dimensions are square ranging from 0.5 mm to 1 mm in length/width/depth and circle ranging from 0.5 mm to 1 mm in diameter/depth. The width/height dimensions are taken from the study [18]. These features are visible using the Zeiss Stereo discovery V20 optical microscope [18]. This designed is inspired from the pre-existing benchmark shown in fig (14B).

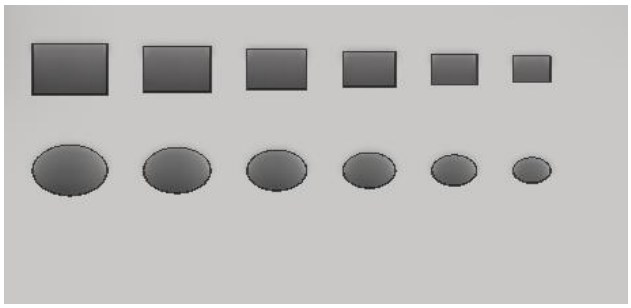

Figure 44 Intrusion geometry (square and circle)

Helical channel: This designed is inspired from the microfluidic with helical channels shown in the fig 15. They aid in the particle sorting applications of microfluidics as they are characterized by a geometry that is defined as a curve winding channel around a center point with continuous decreasing or increasing manner. The flow that passes through the curvature, creates a velocity mismatch in the curve section of this channel, thereby generating secondary flows [26].

i) Nonplanar helical channel at midway length with diameter 1 mm throughout the width 28 mm (fig (48)). The channel is placed at the midway for better visualization of the flow inside.

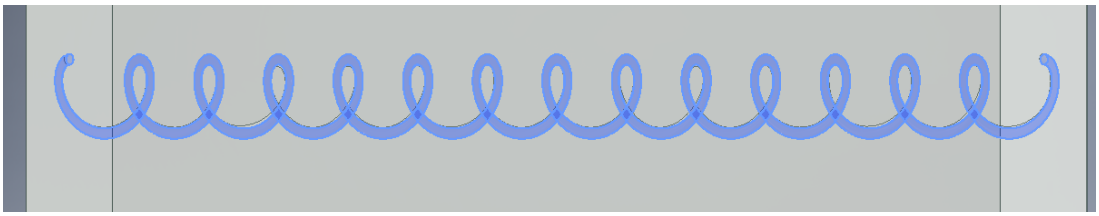

Figure 45 Helical channel with a circular cross-section

Non-planar circular channels with T and Y junction (Fig 49): The Nonplanar channels, when used at higher Re, induce an inertial focusing, thereby can be lending their way in several applications. This is placed at the corner for the same reason as the helical channel, for better visualization of the flow inside the channels. The fig (49) shows three inlet channels and one outlet channel with dimensions 500 and 1000 μm, respectively. To check the feasibility and the manufacturability of the DLP machine we chose these dimensions. Also, manufacturing of these nonplanar channels is new on the selected DLP machine.

Figure 46 Non-planar circular channels with T and Y junction

j) Complex 3-dimensional nonplanar channel (Fig 50): the 3D non-planar channels used to form the emulsion that can be used in drugs and cosmetics, inspired from the fig 17 [40]. The complex 3D channel used in the separation of the blood samples. These channels gradually decrease in size, channel height, and width. Channel is circular with a diameter of 0.5 mm inlet (Fig 52) is at the top and exits at the side (Fig 51) so that the fluid enters and leaves freely. Channel length gradually decreases from 10 mm, 8 mm, and 6 mm also contains several bents to check how the fluid flows in the microfluidic non-planar channels.

For better visualization from all the views, no features are placed near to the complex 3D channels. These complex channels are new and challenging.

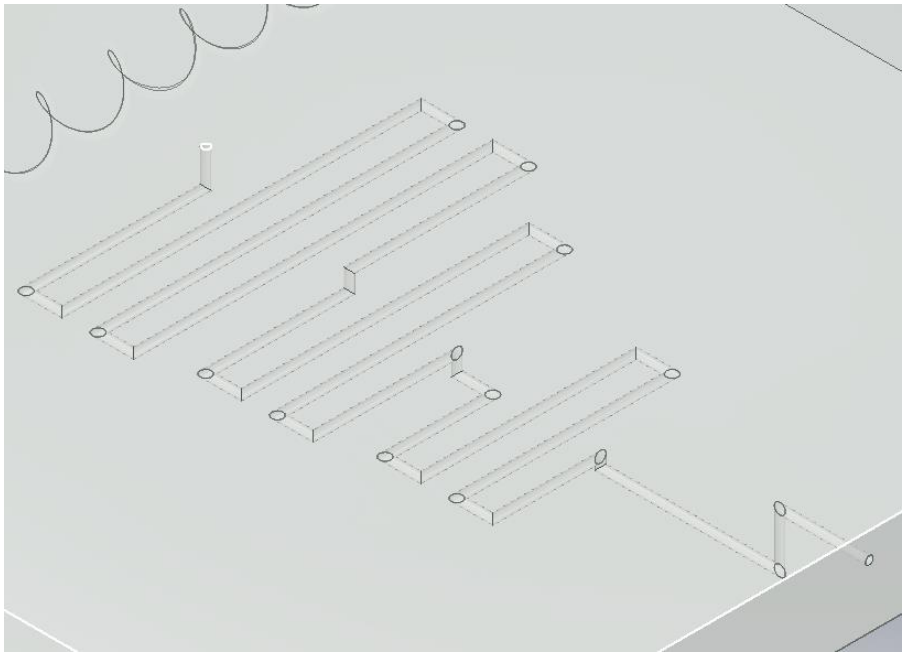

Figure 47 Complex 3D Non-planar circular channel

Both Nonplanar T and Y junctions and the complex 3D channel are new and challenging to manufacture using the selected DLP machine. As said earlier, existing studies [18, 38] shows that the planar channels can be manufactured using the present DLP machine. The manufacturability of the nonplanar channels needed to be investigated.

CHAPTER 4

CONCLUSIONS AND FUTURE DEVELOPMENTS

4. CONCLUSION AND FUTURE DEVELOPMENTS

This research focusses on the need for better technology to the current conventional soft lithography for the manufacturing of Lab-on-a-chip devices (LOC). By narrowing down the research to the Stereolithography processes, and by proper selection of parameters in terms of layer thickness, exposure time, and resin the digital light processing Stereolithography process can be a better alternative solution to the conventional microfluidic fabrication process in terms of cost, space, time, product quality, and biocompatibility.

Several literature reviews on benchmark artifacts along with typical features of microfluidic applications were studied carefully for their design. These designs had several channels with varying geometrical and cross-sectional features, which were the function of their application. Thus, a foundation in the proposition of a new benchmark artifact was laid. The proposed benchmark artifact comprises of planar and nonplanar 3d-channels with varying geometries and cross-sections along with various junctions. Simple geometrical features such as extrusions, intrusions, holes supporting the resolution, and spatial repeatability are also included. Adding to this, the preliminary experimental campaign that was performed on the artifact proposed by a bachelor thesis “studio preliminare della fattibilità dell’ultra-fast prototyping di lab-on-chips mediante stereolitografia” to perform a qualitative analysis and an anova analysis to establish the effect and significance of the process parameters on the feature fabrication and dimension, thereby evaluating the geometrical performance of the digital light processing Stereolithography system.

The further steps of this study will focus on the manufacturing of the designed artifact to perform the experimental campaign to investigate the capability and performance of the digital light processing Stereolithography process for the manufacturing microfeatures for microfluidic devices. Investigations to be made for the selection of most suitable resin for the considered application, and the applicability of complex geometries with complex cross-sections in the field of microfluidics, and thereby, exploiting the digital light processing Stereolithography process to manufacture more complex geometries with complex cross-sections. Also, there is a scope of including much more complex channels and junctions in the artifact. Further, Advance research can be carried out to realize nano-fluidics and its applications, using existing or better technology.

REFERENCES

1. Ho, Chee Meng Benjamin, Sum Huan Ng, King Ho Holden Li, and Yong-Jin Yoon. "3D printed microfluidics for biological applications." Lab on a Chip 15, no. 18 (2015): 3627-3637.
2. Rebaioli, Lara, and Irene Fassi. "Preliminary Study on the Manufacturing Feasibility of Microfeatures for Microfluidics by DLP Stereolithography." In International Design Engineering Technical Conferences and Computers and Information in Engineering Conference, vol. 59223, p. V004T08A015. American Society of Mechanical Engineers, 2019.
3. Waheed, Sidra, Joan M. Cabot, Niall P. Macdonald, Trevor Lewis, Rosanne M. Guijt, Brett Paull, and Michael C. Breadmore. "3D printed microfluidic devices: enablers and barriers." Lab on a Chip 16, no. 11 (2016): 1993-2013.
4. Vaezi, Mohammad, Hermann Seitz, and Shoufeng Yang. "A review on 3D micro-additive manufacturing technologies." The International Journal of Advanced Manufacturing Technology 67, no. 5-8 (2013): 1721-1754.
5. Amin, Reza, Stephanie Knowlton, Alexander Hart, Bekir Yenilmez, Fariba Ghaderinezhad, Sara Katebifar, Michael Messina, Ali Khademhosseini, and Savas Tasoglu. "3D-printed microfluidic devices." Biofabrication 8, no. 2 (2016): 022001.
6. Jiménez, Mariano, Luis Romero, Iris A. Domínguez, María del Mar Espinosa, and Manuel Domínguez. "Additive manufacturing technologies: An overview about 3D printing methods and future prospects." Complexity 2019 (2019).
7. Waheed, Sidra, Joan M. Cabot, Niall P. Macdonald, Trevor Lewis, Rosanne M. Guijt, Brett Paull, and Michael C. Breadmore. "3D printed microfluidic devices: enablers and barriers." Lab on a Chip 16, no. 11 (2016): 1993-2013.
8. Gibson, Ian, David W. Rosen, and Brent Stucker. Additive manufacturing technologies. Vol. 17. New York: Springer, 2014.
9. Herderick, Edward D. "Progress in additive manufacturing." JOM 67, no. 3 (2015): 580-581.
10. Paulo Jorge Bártolo, "Stereolithographic Process" in Paulo Jorge Bártolo, (ed.) Stereolithography Ihsan, Zain Ul. "Projection micro stereolithography apparatus." (2016).
11. Ho, Chee Meng Benjamin, Sum Huan Ng, King Ho Holden Li, and Yong-Jin Yoon. "3D printed microfluidics for biological applications." Lab on a Chip 15, no. 18 (2015): 3627-3637.
12. Beal, V. E., C. H. Ahrens, and P. A. Wendhausen. "The use of stereolithography rapid tools in the manufacturing of metal powder injection molding parts." Journal of the Brazilian Society of Mechanical Sciences and Engineering 26, no. 1 (2004): 40-46.
13. Gardan, Julien. "Additive manufacturing technologies: state of the art and trends." International Journal of Production Research 54, no. 10 (2016): 3118-3132.
14. Bártolo, Paulo Jorge, ed. Stereolithography: materials, processes, and applications. Springer Science & Business Media, 2011.

15. Davis, Brian Edward. "Characterization and calibration of stereolithography products and processes." PhD diss., School of Mechanical Engineering, Georgia Institute of Technology, 2001.
16. Melchels, Ferry PW, Jan Feijen, and Dirk W. Grijpma. "A review on stereolithography and its applications in biomedical engineering." Biomaterials 31, no. 24 (2010): 6121-6130.
17. Ren, Kangning, Jianhua Zhou, and Hongkai Wu. "Materials for microfluidic chip fabrication." Accounts of chemical research 46, no. 11 (2013): 2396-2406.
18. Rebaioli, Lara, and Irene Fassi. "A Benchmark Artifact to Evaluate the Manufacturing of Microfeatures by Digital Light Processing Stereolithography." Journal of Micro and Nano-Manufacturing 8, no. 1 (2020).
19. Nge, Pamela N., Chad I. Rogers, and Adam T. Woolley. "Advances in microfluidic materials, functions, integration, and applications." Chemical reviews 113, no. 4 (2013): 2550-2583.
20. Au, Anthony K., Wonjae Lee, and Albert Folch. "Mail-order microfluidics: evaluation of stereolithography for the production of microfluidic devices." Lab on a Chip 14, no. 7 (2014): 1294-1301.
21. Kanai, Toshimitsu, and Masaki Tsuchiya. "Microfluidic devices fabricated using stereolithography for preparation of monodisperse double emulsions." Chemical Engineering Journal 290 (2016): 400-404.
22. Charles, Guillaume, Thibault Roques-Carmes, Nidhal Becheikh, Laurent Falk, and Serge Corbel. "Impact of the design and the materials of rectangular microchannel reactors on the photocatalytic decomposition of organic pollutant." Green Processing and Synthesis 1, no. 4 (2012): 363-374.
23. Au, Anthony K., Wilson Huynh, Lisa F. Horowitz, and Albert Folch. "3D-printed microfluidics." Angewandte Chemie International Edition 55, no. 12 (2016): 3862-3881.
24. Calvert, Paul, and Robert Crockett. "Chemical solid free-form fabrication: making shapes without molds." Chemistry of materials 9, no. 3 (1997): 650-663.
25. Stampfl, J., M. Schuster, S. Baudis, H. Lichtenegger, R. Liska, C. Turecek, and F. Varga. "Biodegradable stereolithography resins with defined mechanical properties." Virtual and Rapid Manufacturing, Proceedings of VRAP, Leira, Portugal (2007): 283-288.
26. 3D printing: an emerging tool for novel microfluidics and lab-on-a-chip applications, last accessed Dec 2020 https://envisiontec.com/3d-printers/desktop-3d-printers/micro-plus-hi-res.
27. Bazaz, Sajad Razavi, Omid Rouhi, Mohammad Amin Raoufi, Fatemeh Ejeian, Mohsen Asadnia, Dayong Jin, and Majid Ebrahimi Warkiani. "3D Printing of Inertial Microfluidic Devices." Scientific reports 10, no. 1 (2020): 1-14.
28. Kanai, Toshimitsu, and Masaki Tsuchiya. "Microfluidic devices fabricated using stereolithography for preparation of monodisperse double emulsions." Chemical Engineering Journal 290 (2016): 400-404.

29. Kanai, Toshimitsu, Kanako Ohtani, Masafumi Fukuyama, Toru Katakura, and Masatoshi Hayakawa. "Preparation of monodisperse PNIPAM gel particles in a microfluidic device fabricated by stereolithography." Polymer journal 43, no. 12 (2011): 987-990.
30. Fang, Shimeng, Hongzhu Tian, Xiancheng Li, Dong Jin, Xiaojie Li, Jing Kong, Chun Yang et al. "Clinical application of a microfluidic chip for immunocapture and quantification of circulating exosomes to assist breast cancer diagnosis and molecular classification." PLoS One 12, no. 4 (2017): e0175050.
31. Weng, Xuan, Wenting Zhao, Suresh Neethirajan, and Todd Duffield. "Microfluidic biosensor for β-Hydroxybutyrate (βHBA) determination of subclinical ketosis diagnosis." Journal of nanobiotechnology 13, no. 1 (2015): 13.
32. Li, Shunbo, Xiuqing Gong, Ciara S. Mc Nally, Muling Zeng, Thembaninkosi Gaule, Clara Anduix-Canto, Alexander N. Kulak, Lukmaan A. Bawazer, Michael J. McPherson, and Fiona C. Meldrum. "Rapid preparation of highly reliable PDMS double emulsion microfluidic devices." RSC advances 6, no. 31 (2016): 25927-25933.
33. Okushima, Shingo, Takasi Nisisako, Toru Torii, and Toshiro Higuchi. "Controlled production of monodisperse double emulsions by two-step droplet breakup in microfluidic devices." Langmuir 20, no. 23 (2004): 9905-9908.
34. Deshpande, Siddharth, Yaron Caspi, Anna EC Meijering, and Cees Dekker. "Octanol-assisted liposome assembly on chip." Nature communications 7, no. 1 (2016): 1-9.
35. Kim, J-A., J. Lee, C. Wu, S. Nam, Dino Di Carlo, and Wonhee Lee. "Inertial focusing in non-rectangular cross-section microchannels and manipulation of accessible focusing positions." Lab on a Chip 16, no. 6 (2016): 992-1001.
36. Hwang, Yongha, and Rob N. Candler. "Non-planar PDMS microfluidic channels and actuators: a review." Lab on a Chip 17, no. 23 (2017): 3948-3959.
37. Li, Jin, and D. A. Barrow. "A new droplet-forming fluidic junction for the generation of highly compartmentalised capsules." Lab on a Chip 17, no. 16 (2017): 2873-2881.
38. Ludovico Martignoni, Matteo Quadrio, Giada Ravanelli, Federica Rimoldi, Sebastiano Riva, 2019, “studio Studio preliminare della fattibilità dell’ultra-fast prototyping di lab-on-chips mediante stereolitografia”, Politecnico di Milano by Ludovico Martignoni – 866205 Matteo Quadrio – 869054 Giada Ravanelli – 866048 Federica Rimoldi – 867684 Sebastiano Riva – 870223.
39. Morimoto, Yuya, Wei-Heong Tan, and Shoji Takeuchi. "Three-dimensional axisymmetric flow-focusing device using stereolithography." Biomedical microdevices 11, no. 2 (2009): 369-377.
40. Chan, Ho Nam, Yangfan Chen, Yiwei Shu, Yin Chen, Qian Tian, and Hongkai Wu. "Direct, one-step molding of 3D-printed structures for convenient fabrication of truly 3D PDMS microfluidic chips." Microfluidics and nanofluidic 19, no. 1 (2015): 9-18.

APPENDIX

ABBREVATIONS:

Glossary of terms that are used

3D 3 Dimensional

AM Additive manufacturing

SLA Stereolithography

DLP Digital Light processing

2PP Two-photon polymerization

LOC Lab-on-a-chip

FDM Fused Deposition Modelling

PMMA Polymethyl methacrylate

PDMS Polydimethylsiloxane

PC Polycarbonate

NMP N-methyl pyrrolidone

The units of measure for the table are mm. The tests are differentiated based on process parameters, namely exposure time (in milliseconds) and thickness layer (in micrometres).

Table 7: Negative Feature with Circular section (G feature with diameter = 1.5 mm)

Layer Thickness	Exposure Time	error	Measured diameter (mm)
50	7000	-41.88	1.45812
100	7000	36.52	1.53652
150	7000	118.66	1.61866
50	9500	-87.77	1.41223
100	9500	12.025	1.512025
150	9500	13.785	1.513785
50	1200	-64.135	1.435865
100	1200	-5.025	1.494975
150	1200	4.975	1.504975
50	7000	-30.05	1.46995
100	7000	71.6	1.5716
150	7000	114.285	1.614285
50	9500	-159.25	1.34075
100	9500	-16.905	1.483095
150	9500	55.69	1.55569
50	1200	-76.85	1.42315
100	1200	-77.93	1.42207
150	1200	4.135	1.504135

Table 8: Negative Feature with Square section (H feature with width = 1.5 mm)

Layer Thickness	Exposure Time	Error	Measured diameter (mm)
50	7000	-0.288	1.212
100	7000	-0.0905	1.4095
150	7000	0.1145	1.6145
50	9500	-0.185	1.315
150	9500	-0.0235	1.4765
50	1200	0.016	1.516
100	1200	-0.055	1.445
150	1200	-0.1105	1.3895
50	7000	-0.087	1.413
100	7000	0.045	1.545
150	7000	0.072	1.572
50	9500	-0.213	1.287
100	9500	-0.0585	1.4415
150	9500	-0.017	1.483
50	1200	-0.367	1.133
100	1200	-0.3035	1.1965
150	1200	-0.095	1.405

Table 9: Positive Feature with Circular Section (N round feature with diameter = 1.25 mm)

Layer Thickness	Exposure Time	Error	Measured diameter (mm)
50	7000	0.005	1.255
100	7000	0.005	1.255
150	7000	-0.115	1.135
50	9500	0.04	1.29
150	9500	0.005	1.255
50	1200	0.07	1.32
100	1200	0.02	1.27
150	1200	0.02	1.27
50	7000	-0.03	1.22
100	7000	-0.03	1.22
150	7000	-0.085	1.165
50	9500	0.03	1.28
100	9500	0.035	1.285
150	9500	-0.02	1.23
50	1200	0.06	1.31
100	1200	0.025	1.275
150	1200	0.01	1.26

Table 10: Positive Feature with Square Section (N square feature with width = 1.5 mm)

Layer Thickness	Exposure Time	Error	Measured width (mm)
50	7000	-0.015	1.485
100	7000	0	1.5
150	7000	-0.11	1.39
50	9500	0.04	1.54
100	9500	-0.02	1.48
150	9500	-0.005	1.495
50	1200	0.065	1.565
100	1200	0.02	1.52
150	1200	0.005	1.505
50	7000	-0.025	1.475
100	7000	-0.065	1.435
150	7000	-0.06	1.44
50	9500	0.03	1.53
100	9500	0.035	1.535
150	9500	-0.035	1.465
50	1200	0.065	1.565
100	1200	0.025	1.525
150	1200	0.005	1.505